Scalar generalized-screen algorithms in transversely isotropic media with a vertical symmetry axis

JÉRÔME H. LE ROUSSEAU
AND
MAARTEN V. DE HOOP
Center for Wave Phenomena, Colorado School of Mines, Golden CO, USA

October 15, 1999

ABSTRACT

The scalar generalized-screen method in isotropic media is extended here to transversely isotropic media with a vertical symmetry axis (VTI). Although wave propagation in a transversely isotropic medium is essentially elastic, we introduce an equivalent 'acoustic' system of equations for the qP-waves which we prove to be accurate for both the dispersion relation and the polarization angle, in the case of 'mild' anisotropy. The enhanced accuracy of the generalized-screen method as compared to the phase-screen and the split-step Fourier methods allows the extension to VTI media. The generalized-screen expansion of the one-way propagator follows closely the method used in the isotropic case. The medium is defined in terms of a background and a perturbation. The generalized-screen expansion of the vertical slowness is based upon an expansion of the medium parameters simultaneously into magnitude and smoothness of variation. We cast the theory into numerical algorithms. We assess the accuracy of the generalized-screen method in a particular VTI medium with complex structure, viz. the BP Amoco Valhall model, in which multi-pathing is significant.

INTRODUCTION

In realistic geological models, heterogeneity in medium properties is such that the phenomenon of multiple scattering is significant. We distinguish two classes of multiple scattering: one in which the multiples are identified with respect to the projection of their propagation paths onto the *vertical* direction (depth), and one where the multiples are identified with respect to the projection of their propagation paths onto the *horizontal* plane. In the asymptotic framework of wavefront analysis, paths are rays. The *first* class of multiple scattering is associated with 'turning rays' and 'internal multiples' as well as 'surface multiples', the *second*, possibly combined with the first class of multiple scattering, is associated with 'multi-pathing'.

Wave extrapolation methods are able to account for multi-pathing (second class of multiple scattering), with no need to follow the formation of caustics explicitly. However, their computational complexity is significant and hence fast, approximate, algorithms are of interest, in particular in 3D. Methods such as the phase-screen (Ratcliffe, 1956) and the closely related split-step Fourier (Stoffa *et al.*, 1990) methods yield fast 3D algorithms. They are, however, limited in their capacity to predict large-angle propagation where significant lateral heterogeneities are present. Because of their attractive properties (3D, multi-pathing), De Hoop *et al.* (1999) and Le Rousseau and De Hoop (1999) generalized this latter family of algorithms, enhancing their accuracy. With the generalized-screen (GS) approach, the accuracy of the phase-screen method is generalized to larger-contrast, wider-angle, and back-scattering. We propose here to extend the GS method further to anisotropic media, in particular to transversely isotropic media with a vertical symmetry axis (VTI media). The extension of the GS method to media with less symmetry (e.g. orthorhombic) can be accomplished in a similar fashion. The enhanced accuracy accomplished by the GS approach becomes a necessity in the application to VTI media.

Our approach accounts for the *first* class of multiple scattering through use of the generalized Bremmer series (De Hoop, 1996), and for the *second* class of multi-pathing by means

of the GS propagation (De Hoop *et al.*, 1999; Le Rousseau & De Hoop, 1999). Examples of implementation of the Bremmer series with the one-way wave operator approximated with the GS method can be found in Le Rousseau and De Hoop (1999). Here, we only consider the first term of the Bremmer series associated with the one-way wave operator that models transverse scattering.

The propagator that generates the Bremmer series can be represented by a Hamiltonian path integral (De Witte-Morette *et al.*, 1979; Fishman & McCoy, 1984a; Fishman & McCoy, 1984b; De Hoop, 1996) that accounts for not only the energy traveling along the ray but also for the transport along non-stationary paths. These path integrals contain all possible multi-pathing. In the path integral, 'time' is identified with depth, and 'momenta' are identified with the horizontal wave slownesses which, in the ray-theoretic limit, coincide with the horizontal components of the gradient of travel time. The (square-root) Hamiltonian, appearing in the phase of the path integral, is identified with vertical wave slowness. The GS approach yields a fast algorithm for the path integrals.

We analyze the accuracy of the GS method in complex VTI structures using the synthetic BP Amoco VTI Valhall model. This model exhibits significant multi-pathing and is representative of a North Sea geology. In the Valhall model, a so-called 'gas cloud' in the overburden creates a low velocity zone for qP-waves. This geologic situation yields poor imaging below the 'gas cloud' with standard single-path methods using the qP-qP energy. With the help of the GS propagator, which we prove to be accurate in these situations, we shall illustrate that the origin of this problem is possibly associated with multi-pathing.

Wave propagation in VTI media is essentially elastic. Yet, in various applications the propagation of qP-waves only is considered as if the medium were acoustic. Following the work of Schoenberg and De Hoop (1999) we introduce in Appendix A an equivalent 'acoustic' system of equations for VTI qP-wave propagation. We show the accuracy of this equivalent 'acoustic' system for the qP-wave propagation for both the dispersion relation, i.e. the wavefront set, and

the polarization angle. In Appendix B, we follow the procedure introduced by De Hoop (1996) to decompose the wavefield into up- and downgoing components. Doing so, we introduce the vertical slowness operator for the equivalent 'acoustic' medium and give the general form for the one-way wave propagator in such a medium.

We first present the dispersion relation for qP-waves in VTI media and the approximate, yet accurate, simplification introduced by Schoenberg and De Hoop (1999). Starting from that simplified dispersion relation, we derive the GS representation of the thin-slab propagator in VTI media. The results are then cast into a numerical algorithm. We carry out our accuracy analysis through modeling and therefore indirectly analyze the migration operator before stacking that is performed in the process of imaging. We focus on multi-pathing and second-arrival energy.

THE SCALAR GENERALIZED-SCREEN PROPAGATOR IN TRANSVERSELY ISOTROPIC MEDIA WITH A VERTICAL SYMMETRY AXIS

For transversely isotropic (TI) media, the dispersion relation associated with qP-wave propagation is not quite as simple as in the isotropic case (e.g., Le Rousseau & De Hoop, 1999, equation (9)). Because the phase velocity is a function of angle, the slowness surface is not a sphere. Nevertheless, to apply a GS-type expansion (De Hoop *et al.*, 1999; Le Rousseau & De Hoop, 1999) as in the isotropic case, one would like to have a dispersion relation as close as possible to the one of the isotropic case. This is accomplished here using the approximate, yet accurate, dispersion relation in TI media developed by Schoenberg and De Hoop (1999).

Transversely isotropic media with a vertical symmetry axis

Throughout the paper, we shall treat the qP-wave as a scalar wave. In the scalar approximation, we neglect any type of mode conversion. We consider the case of TI media with a vertical symmetry axis (VTI), so without loss of generality one can confine attention to a single vertical plane.

An elastic medium is defined by its stiffness tensor (C_{ijkl}). With the so-called Voigt notation (Thomsen, 1986), one can represent the medium by a 6×6 matrix in accordance with

$$\begin{array}{lcccccc} ij \text{ or } kl: & 11 & 22 & 33 & 32=23 & 31=13 & 12=21\,. \\ & \downarrow & \downarrow & \downarrow & \downarrow & \downarrow & \downarrow \\ & 1 & 2 & 3 & 4 & 5 & 6 \end{array}$$

In the case of a TI medium, the non-vanishing entries are given by

$$\begin{pmatrix} c_{11} & c_{11}-2c_{66} & c_{13} & & & \\ c_{11}-2c_{66} & c_{11} & c_{13} & & & \\ c_{13} & c_{13} & c_{33} & & & \\ & & & c_{55} & & \\ & & & & c_{55} & \\ & & & & & c_{66} \end{pmatrix} . \tag{1}$$

Simplified dispersion relation for qP-wave propagation

We select the direction of preference along the x_3-axis (or 'vertical' axis) and denoting the remaining ('transverse' or 'horizontal') coordinates by x_μ, $\mu = 1, 2$. Terms $\tilde{c}_{ij}$ represent the elastic moduli c_{ij} divided by the density ρ, and thus have dimension velocity squared.

In the present development, it is advantageous to use the Laplace transform with respect to time, t, and the Fourier transform with respect to the horizontal spatial coordinates, x_μ. We introduce the notation

$$s = -\mathrm{i}\omega\,, \tag{2}$$

$$\alpha_\nu = \frac{1}{\mathrm{i}\omega}\,k_\nu = -\frac{1}{s}\,k_\nu\,, \tag{3}$$

where ω and k_ν are the frequency and the horizontal wavenumber components. Let γ_1 be the vertical slowness[1],

$$\gamma_1 = \frac{k_3}{\omega}\,, \tag{4}$$

[1] we explain the subscript 1 in γ_1 in Appendix B

where k_3 is the vertical wavenumber. From the Christoffel equation, associated with equation (1), we have the dispersion relation

$$\tilde{c}_{11}\tilde{c}_{55}(\alpha^2)^2 - \left[(\tilde{c}_{11}+\tilde{c}_{33})\tilde{c}_{55}+E^2\right]\alpha^2\gamma_1^2 + \tilde{c}_{33}\tilde{c}_{55}(\gamma_1^2)^2$$

$$+(\tilde{c}_{11}+\tilde{c}_{55})\alpha^2 - (\tilde{c}_{33}+\tilde{c}_{55})\gamma_1^2 + 1 = 0\,, \tag{5}$$

where

$$E^2 = (\tilde{c}_{11}-\tilde{c}_{55})(\tilde{c}_{33}-\tilde{c}_{55}) - (\tilde{c}_{13}+\tilde{c}_{55})^2\,. \tag{6}$$

We work in a vertical plane without loss of generality and use α instead of α_1 and α_2 ($\alpha^2 = \alpha_\nu\alpha_\nu$). Throughout the paper we use the summation convention for repeated indices. To study the qP-wave behavior, we carry out the change of variables

$$X = -\tilde{c}_{11}\alpha^2\,; \quad Z = \tilde{c}_{33}\gamma_1^2\,. \tag{7}$$

The dispersion relation becomes

$$\frac{\tilde{c}_{55}}{\tilde{c}_{11}}X^2 + \left[\left(\frac{\tilde{c}_{55}}{\tilde{c}_{11}}+\frac{\tilde{c}_{55}}{\tilde{c}_{33}}\right)+\frac{E^2}{\tilde{c}_{11}\tilde{c}_{33}}\right]XZ + \frac{\tilde{c}_{55}}{\tilde{c}_{33}}Z^2 \tag{8}$$

$$-\left(1+\frac{\tilde{c}_{11}}{\tilde{c}_{55}}\right)X - \left(1+\frac{\tilde{c}_{33}}{\tilde{c}_{55}}\right)Z + 1 = 0\,.$$

Schoenberg and De Hoop (1999) rewrite the dispersion relation as

$$Z = 1 - X + f(X, E^2)\,, \tag{9}$$

where f can be expanded in terms of a rational approximation of a factor of the form $X(1-X)$, which ensures accuracy at both normal ($X = 0$) and grazing ($X = 1$) incidence.

Schoenberg and De Hoop (1999) also show a simplification of the qP dispersion relation that turns out quite useful here. The exact solution for the qP slowness depends weakly on $\tilde{c}_{13}$ and $\tilde{c}_{55}$ individually but strongly on $\tilde{a} = \tilde{c}_{13} + 2\tilde{c}_{55}$ in the case of 'mild' anisotropy. Schoenberg and De Hoop (1999) propose then the following transformation

$$\tilde{c}_{13} \to \tilde{a}\,,\ \tilde{c}_{55} \to 0\,. \tag{10}$$

In this limit, equation (8) simplifies to

$$\left[1-\left(1-\frac{\tilde{a}^2}{\tilde{c}_{11}\tilde{c}_{33}}\right)X\right]Z=1-X\ , \tag{11}$$

which is an exact rational representation of Z. Schoenberg and De Hoop (1999) show that this latter approximation is accurate even for slownesses that are between normal and grazing incidence. More generally, this limit (10) can be applied to the vector wave equation as is done in Appendix A. There we show that not only is the approximation proposed by Schoenberg and De Hoop (1999) accurate for the dispersion relation, i.e. for the wavefront set, but also for the polarization vector of the qP-waves.

If we introduce Thomsen's parameters ε and δ (Thomsen, 1986)

$$\varepsilon=\frac{c_{11}-c_{33}}{2c_{33}}\ ,$$

$$\delta=\frac{(c_{13}+c_{55})^2-(c_{33}-c_{55})^2}{2c_{33}(c_{33}-c_{55})}\ ,$$

with δ becoming

$$\delta=\frac{a^2-c_{33}^2}{2c_{33}^2}\ ,$$

in the frame of the limit (10), and use c_V as the vertical qP-wave wave speed, i.e.,

$$c_V=\sqrt{\tilde{c}_{33}}\ ,$$

relation (11) becomes

$$\gamma_1^2=c_V^{-2}\frac{1+c_V^2\alpha^2(1+2\varepsilon)}{1-2c_V^2\alpha^2(\delta-\varepsilon)}\ , \tag{12}$$

which, away from a vertical plane, can be written as

$$\gamma_1(\boldsymbol{x};\alpha_\nu)=\sqrt{[c_V(\boldsymbol{x})]^{-2}\ \frac{1+[c_V(\boldsymbol{x})]^2\ \alpha_\nu\alpha_\nu\ [1+2\varepsilon(\boldsymbol{x})]}{1-2[c_V(\boldsymbol{x})]^2\ \alpha_\nu\alpha_\nu\ [\delta(\boldsymbol{x})-\varepsilon(\boldsymbol{x})]}}\ . \tag{13}$$

Note that letting ε and δ go to zero leads to the dispersion equation in the isotropic case (e.g., Le Rousseau & De Hoop, 1999), as it should. The vector $(\mathrm{i}\alpha_1,\mathrm{i}\alpha_2,\gamma_1)$ is the gradient of travel time consistent with the eikonal equation. We use the dispersion relation (13) to derive the anisotropic scalar one-way propagator.

The scalar one-way propagator

For a sufficiently small vertical step Δx_3, and a medium sufficiently smooth, the Hamiltonian path-integral representation for the one-way thin-slab propagator reduces to (De Hoop *et al.*, 1999):

$$g^{(\pm)}(x_\mu, x_3; x'_\upsilon, x'_3) \simeq$$

$$\int (s/2\pi)^2 \mathrm{d}\alpha_1 \mathrm{d}\alpha_2 \exp[-\mathrm{i}s\,\alpha_\sigma(x_\sigma - x'_\sigma)] \exp[\mp s\,\gamma_1(x_\mu, \bar{x}_3; \alpha_\nu)\Delta x_3] \;, \qquad (14)$$

with

$$\Delta x_3 = x_3 - x'_3 \;,$$

$$\bar{x}_3 = x_3 - \tfrac{1}{2}\Delta x_3 = x'_3 + \tfrac{1}{2}\Delta x_3 \;,$$

and where γ_1 is given by the dispersion relation (13). Here, we have used a 'high-frequency' approximation, i.e. we assume the medium to be locally constant. Appendix A introduces an equivalent 'acoustic' system for the elastic propagation of qP-waves in VTI media. In Appendix B we work out the wavefield decomposition from this equivalent 'acoustic' system as it is done in the isotropic case (De Hoop, 1996). Also, we show that $gamma_1$ has the interpretation of the symbol of the principal part of the vertical slowness operator. Then the expression of the one-way wave propagation follows the same as in the isotropic case, hence the form of equation (14).

In the limit of a laterally homogeneous thin slab, γ_1 will not depend on x_μ, and the thin-slab propagator reduces to Gazdag's phase-shift operator, introduced in the isotropic case (Gazdag, 1978). The operator is composed of a forward Fourier transform, a multiplication by a phase factor (the phase is proportional to the vertical slowness) and an inverse Fourier transform. In the general case of equation (14), the thin-slab propagator has a similar structure except that the phase factor is dependent upon the output point, x_μ. Every output point requires its

own evaluation of equation (14), which represents a considerable computational effort. The GS approximation of the thin-slab propagator enforces a simplification of this computational complexity, while allowing laterally varying media.

Generalized-screen principal-slowness surface

Medium parameterization and contrast formulation.—For the subsequent analysis, we employ a 'contrast formulation' that allows us to take lateral heterogeneity into account in the thin-slab propagation. In the slab $[x_3', x_3]$ we introduce a background medium with vertical medium wave speed, c_V^0, and the two Thomsen parameters ε^0 and δ^0. The background medium is constant in the slab, but may vary from one slab to another. We then introduce a triplet of medium perturbations:

$$u(x_\mu, x_3) = [c_V(x_\mu, x_3)]^{-2} - [c_V^0(x_3)]^{-2} , \tag{15}$$

$$u_\varepsilon(x_\mu, x_3) = \varepsilon(x_\mu, x_3) - \varepsilon^0(x_3) , \tag{16}$$

$$u_\delta(x_\mu, x_3) = \delta(x_\mu, x_3) - \delta^0(x_3) . \tag{17}$$

We will expand the vertical slowness left principal symbol, γ_1, into the perturbations u, u_ε, and u_δ, about the background medium.

Generalized-screen expansion.—Assuming small vertical medium variation across the thin slab, i.e., the thin slab is sufficiently small, we set

$$\begin{aligned}\gamma^0(\zeta; \alpha_\nu) &= \sqrt{[c_V^0]^{-2} \frac{1 + [c_V^0]^2 \alpha_\nu \alpha_\nu (1 + 2\varepsilon^0)}{1 - 2[c_V^0]^2 \alpha_\nu \alpha_\nu (\delta^0 - \varepsilon^0)}} \\ &= \gamma^0(x_3; \alpha_\nu) \ \text{ if } \ \zeta \in [x_3', x_3] .\end{aligned} \tag{18}$$

The principal symbol of the vertical slowness, γ_1, will be expanded in u, u_ε, and u_δ. This can be done, for instance, by first expanding γ_1 in u, then in u_ε, and finally in u_δ. The principal

symbol of the vertical slowness, γ_1, can be decomposed into a background term, γ^0, and a perturbation, γ_1^1,

$$\gamma_1(x_\mu, x_3; \alpha_\nu) = \gamma^0(x_3; \alpha_\nu) + \gamma_1^1(x_\mu, x_3; \alpha_\nu) \ . \tag{19}$$

When expanding in the three variables u, u_ε, and u_δ simultaneously, we discard terms that contains products of perturbation terms. We justify this approximation by recognizing that the primary deformation of the slowness surface is caused by the perturbation in the medium slowness squared; variations in the anisotropy parameters are of higher order. This yields the form,

$$\gamma_1^1 \simeq \gamma_u^1 + \gamma_{u_\varepsilon}^1 + \gamma_{u_\delta}^1 \ , \tag{20}$$

where γ_u^1, $\gamma_{u_\varepsilon}^1$, and $\gamma_{u_\delta}^1$ follow the general structures

$$\gamma_u^1(x_\mu, x_3; \alpha_\nu) = \sum_{j=1}^{n_u} \psi_j(x_3; \alpha_\nu) \, [u(x_\mu, x_3)]^j \ , \tag{21}$$

$$\gamma_{u_\varepsilon}^1(x_\mu, x_3; \alpha_\nu) = \sum_{j=1}^{n_{u_\varepsilon}} \psi_{\varepsilon,j}(x_3; \alpha_\nu) \, [u_\varepsilon(x_\mu, x_3)]^j \ , \tag{22}$$

$$\gamma_{u_\delta}^1(x_\mu, x_3; \alpha_\nu) = \sum_{j=1}^{n_{u_\delta}} \psi_{\delta,j}(x_3; \alpha_\nu) \, [u_\delta(x_\mu, x_3)]^j \ . \tag{23}$$

In practice, we limit ourselves to an expansion up to the first order in the anisotropy-parameter perturbations ($n_{u_\varepsilon} = n_{u_\delta} = 1$) , and to fourth order in the squared-slowness perturbation ($n_u \leq 4$) compatible with the isotropic case (Le Rousseau & De Hoop, 1999, equation (18)). Here, the use of equation (13) is particularly fruitful for it avoids use of intricate formulas for the different terms of the GS expansion. The first-order expansions in each perturbation are given by

$$\gamma_u^1(x_\mu, x_3; \alpha_\nu) = u(x_\mu, x_3) \left[\frac{1 - 4[c_V^0(x_3)]^2 \alpha_\nu \alpha_\nu (\delta^0(x_3) - \varepsilon^0(x_3))}{\sigma(x_3; \alpha_\nu)} \right. \tag{24}$$

$$-\frac{2[c_V^0(x_3)]^4(\alpha_\nu\alpha_\nu)^2(\delta^0(x_3)-\varepsilon^0(x_3))(1+2\varepsilon^0(x_3))}{\sigma(x_3;\alpha_\nu)}\Bigg] ,$$

$$\gamma^1_{u_\varepsilon}(x_\mu,x_3;\alpha_\nu)=u_\varepsilon(x_\mu,x_3)\,\frac{[c_V^0(x_3)]^2(\alpha_\nu\alpha_\nu)^2(1+2\delta^0(x_3))}{\sigma(x_3;\alpha_\nu)} , \tag{25}$$

$$\gamma^1_{u_\delta}(x_\mu,x_3;\alpha_\nu)=u_\delta(x_\mu,x_3)\,\frac{[c_V^0(x_3)]^2\alpha_\nu\alpha_\nu\gamma^0(x_3;\alpha_\nu)}{1-2[c_V^0(x_3)]^2\alpha_\nu\alpha_\nu(\delta^0(x_3)-\varepsilon^0(x_3))} , \tag{26}$$

where

$$\sigma(x_3;\alpha_\nu)=2\left(1-2[c_V^0(x_3)]^2\alpha_\nu\alpha_\nu(\delta^0(x_3)-\varepsilon^0(x_3))\right)^2\gamma^0(x_3;\alpha_\nu) \tag{27}$$

Note that, for each of these terms in equation (21) through (23), dependencies on x_μ and α_ν are separated. As in the isotropic case (Le Rousseau & De Hoop, 1999), this property induces the structure of the GS propagator.

The accuracy of each term, γ^1_u, $\gamma^1_{u_\varepsilon}$, and $\gamma^1_{u_\delta}$, can be considered independently. The expansion term γ^1_u provides the same accuracy as its counterpart γ^1_1 in the isotropic case (Le Rousseau & De Hoop, 1999, equation (16)). Figure 1 and Figure 2 illustrate the increasing accuracy of the GS expansion of the vertical slowness principal symbol (γ_1 as a function of the horizontal slowness $p=\sqrt{-\alpha_\nu\alpha_\nu}$) in the contrast in medium slowness squared, u. In Figure 1 the medium is characterized by elliptic anisotropy, i.e., $\varepsilon=\delta$. In Figure 2 the medium is anelliptic (here $\varepsilon=0.2$ and $\delta=0.0$). Adding higher-order terms in the GS expansion (in the medium slowness squared perturbation, u), the shape of the slowness surface is improved, as it is in the isotropic case (Le Rousseau & De Hoop, 1999).

A first-order expansion in the perturbation u_ε in ε proves to be sufficiently accurate, as illustrated in Figure 3, where the contrast between the actual ε and the background ε^0 is 0.2. The behavior of the GS expansion for the perturbation in δ shows surprising accuracy, as illustrated by Figure 4. Although the contrast between the actual local and the background value is 0.2, the GS expansion shows a close to perfect result. One can see that the horizontal propagation is exact. For all practical purposes, the leading term is sufficiently accurate. The accuracy is

due to the fact that in equation (13), δ appears in the denominator. This avoids the creation of a branch point when expanding in u_δ (see below).

Unlike the generalized screens, the split-step-Fourier type approximation (Stoffa *et al.*, 1990) does not have the degree of freedom to account for anisotropy or to shape the slowness surface appropriately. Le Rousseau and De Hoop (1999) show that the split-step Fourier method is accurate only for near-vertical propagation. The influence of the anisotropic parameters (e.g. ε and δ) in the vertical slowness symbol occurs only at non-vertical propagation. As mentioned before, variations in the anisotropy parameters are of higher order than variations in the medium slowness squared, c_V^{-2}. The influence of the anisotropy parameters is comparable to the higher-order terms of the GS expansion that are absent in the split-step Fourier formulation (Le Rousseau & De Hoop, 1999; Thomsen, 1998). In laterally varying medium, taking anisotropy into account in the frame of the Split-step Fourier approximation does not enhance the accuracy of the vertical slowness principal symbol, γ_1, and ,hence , of the associated propagator (cf. next section and Le Rousseau and De Hoop (1999)).

The explicit GS expansion as shown in equations (25) and (26) reveals the introduction of reciprocal powers of γ^0 and hence contains branch points at $\alpha_\nu\alpha_\nu = -[c_V^0]^{-2}/(1+2\varepsilon^0)$. The vicinity of the branch point should be treated carefully. We refer the reader to Le Rousseau and De Hoop (1999) for the treatment of branch points. To ensure that the branch point is out of the propagating regime within the thin-slab, one has to choose c_V^0 smaller than the minimum medium vertical wave speed, and to choose ε^0 smaller than the minimum ε, within the slab as illustrated in Figures 1 through 3.

The scalar generalized-screen propagator VTI media

We have seen that the GS expansion of the slowness surface in the VTI case is quite similar to the one in the isotropic case. The GS expansion of the propagator is hence similar as well,

$$g^{(\pm)}(x_\mu, x_3; x'_\upsilon, x'_3) \simeq \int (s/2\pi)^2 \mathrm{d}\alpha_1 \mathrm{d}\alpha_2 \exp[-\mathrm{i}s\,\alpha_\sigma(x_\sigma - x'_\sigma)] \tag{28}$$

$$\cdot \exp[\mp s \{\gamma^0(\bar{x}_3;\alpha_\nu) + \gamma_u^1(x_\mu,\bar{x}_3;\alpha_\nu) + \gamma_{u_\varepsilon}^1(x_\mu,\bar{x}_3;\alpha_\nu) + \gamma_{u_\delta}^1(x_\mu,\bar{x}_3;\alpha_\nu)\} \Delta x_3] \ .$$

As in the isotropic case, we perform the expansion of the exponential in γ_u^1 about vertical propagation (Le Rousseau & De Hoop, 1999, equation (24)). For the two additional terms, $\gamma_{u_\varepsilon}^1$ and $\gamma_{u_\delta}^1$, the expansion of the exponential simplifies because these terms vanish at vertical propagation. One can thus decompose the propagator as

$$g^{(\pm)} \simeq g^{0(\pm)} + g^{u(\pm)} + g^{u_\varepsilon(\pm)} + g^{u_\delta(\pm)} \ , \tag{29}$$

where cross terms have been discarded when expanding the exponential in γ_u^1. The first term is

$$g^{0(\pm)}(x_\mu,x_3;x'_\upsilon,x'_3) = \exp\left[\mp s \left([c_V(x_\mu,\bar{x}_3)]^{-1} - [c_V^0(\bar{x}_3)]^{-1}\right) \Delta x_3\right] \tag{30}$$

$$\cdot \int (s/2\pi)^2 \mathrm{d}\alpha_1 \mathrm{d}\alpha_2 \exp[-\mathrm{i}s\,\alpha_\sigma(x_\sigma - x'_\sigma)] \ \exp[\mp s\,\gamma^0(\bar{x}_3;\alpha_\nu)\,\Delta x_3] \ ,$$

with γ^0 given by equation (18). The correction applied in the space domain corrects for vertical propagation only. All contributions, $g^{u(\pm)}$, $g^{u_\varepsilon(\pm)}$, $g^{u_\delta(\pm)}$ have the same form; for $g^{u(\pm)}$ we have

$$g^{u(\pm)}(x_\mu,x_3;x'_\upsilon,x'_3) = \exp\left[\mp s \left([c_V(x_\mu,\bar{x}_3)]^{-1} - [c_V^0(\bar{x}_3)]^{-1}\right) \Delta x_3\right] \tag{31}$$

$$\cdot \int (s/2\pi)^2 \mathrm{d}\alpha_1 \mathrm{d}\alpha_2 \Delta x_3 \exp[-\mathrm{i}s\,\alpha_\sigma(x_\sigma - x'_\sigma)] \ \exp[\mp s\,\gamma^0(\bar{x}_3;\alpha_\nu)\,\Delta x_3]$$

$$\cdot \mp s\Delta x_3 \ \left[\gamma_u^1(x_\mu,\bar{x}_3;\alpha_\nu) - \gamma_u^1(x_\mu,\bar{x}_3;0)\right] \ ,$$

which gives, by substituting equation (21),

$$g^{u(\pm)}(x_\mu,x_3;x'_\upsilon,x'_3) = \mp s\Delta x_3 \exp\left[\mp s \left([c_V(x_\mu,\bar{x}_3)]^{-1} - [c_V^0(\bar{x}_3)]^{-1}\right) \Delta x_3\right] \tag{32}$$

$$\cdot \sum_{j=1}^{n_u} \Bigg\{ [u(x_\mu,\bar{x}_3)]^j \int (s/2\pi)^2 \mathrm{d}\alpha_1 \mathrm{d}\alpha_2 \Delta x_3 \exp[-\mathrm{i}s\,\alpha_\sigma(x_\sigma - x'_\sigma)]$$

$$\cdot \exp[\mp s\,\gamma^0(\bar{x}_3;\alpha_\nu)\,\Delta x_3] \ [(\psi_j(\bar{x}_3;\alpha_\nu) - \psi_j(\bar{x}_3;0)] \Bigg\} \ .$$

For the term $g^{u_\varepsilon(\pm)}$, $[\gamma_u^1(x_\mu,\bar{x}_3;\alpha_\nu)-\gamma_u^1(x_\mu,\bar{x}_3;0)]$ should be replaced by $\gamma_{u_\varepsilon}^1(x_\mu,\bar{x}_3;\alpha_\nu)$ and yield

$$g^{u_\varepsilon(\pm)}(x_\mu,x_3;x'_\upsilon,x'_3)=\exp\left[\mp s\,\left([c_V(x_\mu,\bar{x}_3)]^{-1}-[c_V^0(\bar{x}_3)]^{-1}\right)\,\Delta x_3\right] \tag{33}$$
$$\cdot\int(s/2\pi)^2\mathrm{d}\alpha_1\mathrm{d}\alpha_2\Delta x_3\exp[\mathrm{i}s\,\alpha_\sigma(x_\sigma-x'_\sigma)]\;\exp[-\mp s\,\gamma^0(\bar{x}_3;\alpha_\nu)\,\Delta x_3]$$
$$\cdot\mp s\Delta x_3\;\gamma_{u_\varepsilon}^1(x_\mu,\bar{x}_3;\alpha_\nu)\;,$$

which gives, by substituting equation (22),

$$g^{u_\varepsilon(\pm)}(x_\mu,x_3;x'_\upsilon,x'_3)=\mp s\Delta x_3\exp\left[\mp s\,\left([c_V(x_\mu,\bar{x}_3)]^{-1}-[c_V^0(\bar{x}_3)]^{-1}\right)\,\Delta x_3\right] \tag{34}$$
$$\cdot\sum_{j=1}^{n_{u_\varepsilon}}\Bigg\{[u_\varepsilon(x_\mu,\bar{x}_3)]^j\int(s/2\pi)^2\mathrm{d}\alpha_1\mathrm{d}\alpha_2\Delta x_3\exp[-\mathrm{i}s\,\alpha_\sigma(x_\sigma-x'_\sigma)]$$
$$\cdot\exp[\mp s\,\gamma^0(\bar{x}_3;\alpha_\nu)\,\Delta x_3]\;\psi_{\varepsilon,j}(\bar{x}_3;\alpha_\nu)\Bigg\}\;.$$

For the term $g^{u_\delta(\pm)}$, $[\gamma_u^1(x_\mu,\bar{x}_3;\alpha_\nu)-\gamma_u^1(x_\mu,\bar{x}_3;0)]$ should be replaced by $\gamma_{u_\delta}^1(x_\mu,\bar{x}_3;\alpha_\nu)$. In each case, the spatial dependency of the propagator can be taken out of the integral, since it has been separated from the wavenumber dependency via the GS expansion. The GS algorithm in the VTI case therefore has the same structure as in the isotropic case (Le Rousseau & De Hoop, 1999). The additional cost as compared with the isotropic GS algorithm is of the order of two additional inverse Fourier transforms for the first-order terms in u_ε and u_δ.

Figure 5 and Figure 6 show the (instantaneous) wavefronts associated to the slowness surfaces shown in Figure 1 and Figure 2 respectively. Figure 7 and Figure 8 are associated with Figure 3 and Figure 4. Figures 5 through 8 also show the numerical response of the GS propagator in VTI media in such constant-perturbation medium.

As the *computational complexity* of a Fourier transform is $N_1N_2\log_2(N_1N_2)$ (N_μ denoting the numbers of samples in the x_μ-direction), the complexity of our n^{th}-order GS algorithm is proportional to $(2+n)N_1N_2\log_2(N_1N_2)$, where n is the cumulative order of the GS expansion

in the three perturbation terms (u, u_ε, and u_δ), i.e., $n = n_u + n_{u_\varepsilon} + n_{u_\delta}$. Again, in most practical cases, taking $n_{u_\varepsilon} = n_{u_\delta} = 1$ provides sufficient accuracy; then the computational complexity of the GS method is $(4 + n_u)N_1N_2 \log_2(N_1N_2)$.

THE SCALAR GENERALIZED-SCREEN ALGORITHM

Here, we discuss the GS algorithm based upon equations (30) through (34). We denote the (one-way) wavefield by W, and carry out the wave propagation in the frequency domain, with each frequency component computed independently. The downward continuation for modeling and imaging with the one-way propagator is performed according to the decomposition of the vertical slowness symbol into one background term and a series of perturbation terms as in equations (21) through (23).

Let the current depth be set to $x_3' = z$, and set $\bar{x}_3 = x_3' + \frac{1}{2}\Delta x_3$ as before. Following equations (32) and (34), we introduce the intermediate field quantities $w_0, w_1, \cdots, w_n$, and w_ε, and w_δ according to (*step 1*)

$$w_0(x_\mu, s) = \exp\left[-s\,\Delta x_3\,\left([c_V(x_\mu, \bar{x}_3)]^{-1} - [c_V^0(\bar{x}_3)]^{-1}\right)\right]\; W(x_\mu, x_3', s)\;,$$

$$w_1(x_\mu, s) = -s\,\Delta x_3\; u(x_\mu, \bar{x}_3)\; w_0(x_\mu, s)\;,$$

$$w_2(x_\mu, s) = -s\,\Delta x_3\; u^2(x_\mu, \bar{x}_3)\; w_0(x_\mu, s)\;,$$

$$\vdots$$

$$w_n(x_\mu, s) = -s\,\Delta x_3\; u^n(x_\mu, \bar{x}_3)\; w_0(x_\mu, s)\;,$$

$$w_\varepsilon(x_\mu, s) = -s\,\Delta x_3\; u_\varepsilon(x_\mu, \bar{x}_3)\; w_0(x_\mu, s)\;,$$

$$w_\delta(x_\mu, s) = -s\,\Delta x_3\; u_\delta(x_\mu, \bar{x}_3)\; w_0(x_\mu, s)\;.$$

The higher-order terms in u, u_ε, and u_δ increase the accuracy for wider-angle propagation. Again, for practical purposes, we limit ourselves to first-order expansion of the principal slow-

ness symbols in Thomsen parameter perturbations , u_ε and u_δ. The intermediate field quantities are then Fourier transformed to the horizontal-wavenumber domain (*step 2*),

$$\tilde{w}_j(\alpha_\nu, s) = \tilde{w}_j(k_\nu/s, s) = \int w_j(x_\mu, s)\ \exp\left[-\mathrm{i}x_\sigma k_\sigma\right]\ dx_\mu \tag{35}$$

$$= \int w_j(x_\mu, s)\ \exp\left[\mathrm{i}s x_\sigma \alpha_\sigma\right] dx_\mu\ , \qquad j = 0, 1, \cdots, n, \varepsilon, \delta\ .$$

The wavefield at depth $x_3 = z + \Delta x_3$ then follows as

$$\begin{aligned}\tilde{W}(x_3; \alpha_\nu, s) &= \tilde{w}_0(\alpha_\nu, s)\ \exp[-s\Delta x_3 \gamma^0(\bar{x}_3; \alpha_\nu)] \\ &\cdot \mathcal{N}\left[1 + \frac{\tilde{w}_1(\alpha_\nu, s)}{\tilde{w}_0(\alpha_\nu, s)}\ [\psi_1(\alpha_\nu, s) - \psi_1(0, s)]\right. \\ &\quad + \cdots + \frac{\tilde{w}_n(\alpha_\nu, s)}{\tilde{w}_0(\alpha_\nu, s)}\ [\psi_n(\alpha_\nu, s) - \psi_n(0, s)] \\ &\quad \left. + \frac{\tilde{w}_\varepsilon(\alpha_\nu, s)}{\tilde{w}_0(\alpha_\nu, s)}\ \psi_\varepsilon(\alpha_\nu, s) + \frac{\tilde{w}_\delta(\alpha_\nu, s)}{\tilde{w}_0(\alpha_\nu, s)}\ \psi_\delta(\alpha_\nu, s)\right]\ ,\end{aligned}$$

(*step 3*), the divisions being carried out in some stable sense, and the normalization operator, $\mathcal{N}$, being given by

$$\mathcal{N}[1 + p + \mathrm{i}q] = \exp(\mathrm{i}q)\ \left|1 + \frac{p}{1 + \mathrm{i}q}\right|^{-1} \left[1 + \frac{p}{1 + \mathrm{i}q}\right]\ .$$

The Taylor expansion of the exponential in equation (28) destroys the unitarity of the thin-slab propagator, hence the introduction of the normalization operator (Le Rousseau & De Hoop, 1999). Finally, we carry out the inverse Fourier transform $\tilde{W}(x_3; \alpha_\nu, s) \rightarrow W(x_\mu, x_3; s)$ (*step 4*).

ACCURACY ANALYSIS

We illustrate the accuracy of the GS algorithm with the BP Amoco VTI Valhall model. We base our analysis on numerical modeling. We generate Green's functions and focus our observations on second-arrival energy and multi-pathing. Imaging invokes an averaging (stacking) process; to learn about the prestack migration operator, we hence favor to analyze modeling

instead. Depth-migration results for the isotropic case are, however, presented in a companion paper (Le Rousseau & De Hoop, 1999).

The wave speed model (vertical wave speed for qP-waves) of the VTI Valhall model is illustrated in Figure 9. This model, created by BP Amoco (Brandsberg-Dahl *et al.*, 1999), is based on real data studies on the Valhall field in the North Sea. Because of the presence of gas in the overburden of the reservoir, attenuation and multi-pathing occur which yields poor imaging of the qP-waves for conventional asymptotic methods (first arrivals or maximum energy arrivals). 'Gas clouds' act as a dissipative and low wave-speed zone for the qP-waves. Alternative methods, such as imaging using converted waves, have been applied to obtain a better imaging (Thomsen *et al.*, 1997). The qS waves are indeed not affected by the presence of gas. Profiles for Thomsen's parameters ε and δ in the present Valhall model is VTI (Brandsberg-Dahl *et al.*, 1999) are shown in Figure 10 and Figure 11, respectively. The model shows fine detail in the vertical wave speed.

We place a point source beneath the reservoir. The source location is represented by an asterisk in Figure 9. The source is excited at time t $= 0$. The propagating 'pressure' field is imaged at time t = 1.6 s. We compare results generated with the full elastic wave equation (finite-difference time-domain, fourth order in space, second order in time) modeling (Figure 12) with the GS (second order in the perturbation in the vertical slowness squared and first order in the perturbation in ε and δ) method (Figure 13). We use the wavefield modeled by the full elastic wave equation as a reference. The ε section exhibits not so 'weak' anisotropy in parts of the model: ε reaches values as high as 0.3. Yet, the dispersion relation (11) used in VTI media for the GS method is accurate, since it requires 'mild' and not 'weak' anisotropy (Schoenberg & De Hoop, 1999).

The wavefront in the finite-difference section shows significant multi-pathing at various locations, due to lateral variations in the medium properties, especially due to the 'gas cloud', i.e. 'gaz lens'. Also, one can notice significant multiple scattering due to the fine layering of

the model. Comparison with Figure 13 shows the capacity of the GS method to accurately model wave propagation in a non-trivial medium. The wavefront of the GS method closely approaches the reference one. Note that second-arrival energy is accurately positioned. The better positioning and modeling of the latter-arrival energy constitutes a key contribution to the imaging of complex structures, where these arrivals carry a significant part of the energy. We do not address the question of attenuation due to the gas cloud here, though attenuation can be accounted for in the GS approach.

DISCUSSION

The generalized-screen (GS) method is based on the decomposition of the medium into a background component and a perturbation. The GS method can accommodate more significant and rapid horizontal wave speed variations. Its enhanced accuracy (as compared to the phase-screen and split-step method) allows a accurate modeling of the wavefields in complex structures where multi-pathing is significant. Unlike the phase-screen and split-step methods, the GS method extends to media with less symmetry, such as transversely isotropic media with a vertical axis of symmetry (VTI). The medium is then characterized with additional parameters (e.g. Thomsen's parameters ε and δ (Thomsen, 1986)), for which background and perturbation terms are defined. Expansion with respect to the anisotropy parameter perturbation terms are truncated to their lowest order term for this accuracy is sufficient in most practical applications.

With the GS representation of the propagator is associated a symbol, where the dependencies on the spatial coordinates and the dependencies on the wavenumber are factorized -which induces the structure of the GS propagator. The GS expansion provides a fundamental simplification of the one-way propagator. We obtain an algorithm that works as a shuttling between the frequency-horizontal space domain and the frequency-horizontal wavenumber domain. Each new term in the GS expansion increases the accuracy. The additional cost is an additional Fourier transform for each additional order in the expansion (in the perturbation in the medium

slowness squared and the anisotropic parameters). The extension of the GS algorithm to media with less symmetry (e.g. orthorhombic) can be accomplished in a similar fashion.

We have illustrated the GS propagator's accuracy primarily through modeling. The mathematical accuracy analysis of the GS approximation was carried out by De Hoop *et al.* (1999). Here we focus on its numerical counterpart. We chose the BP Amoco VTI Valhall model as a synthetic model representative of a geologic situation. We focused on the computation of Green's functions rather than on imaging because, doing so, we do not hide any details in a prestack migration operator; imaging involves an averaging of these details. The extension of the GS method to VTI yields the expected accuracy. The wavefront modeled with the GS method approaches closely the true one even for second-arrival energy due to multi-pathing in complex structures.

The GS method, with its $(4+n_u)N_1N_2\log_2(N_1N_2)$ (n_u is the order of the GS approximation in the medium slowness squared perturbation, u, and N_μ are the numbers of samples in the horizontal directions) computational complexity, makes feasible 'wave equation' modeling and imaging in 3D VTI media.

ACKNOWLEDGMENTS

The authors would especially like to thank Elf Exploration Production for financial support of this research. We also would like to thank BP Amoco for letting us use their VTI Valhall model. We also would like to thank Henri Calandra for numerous discussions. We would like to thank Alberto Villarreal (Center for Wave Phenomena, Colorado School of Mines) for the use of his finite-difference elastic modeling code in anisotropic media. This work was supported in part by the members of the Consortium Project on Seismic Inverse Methods for Complex Structures at the Center for Wave Phenomena, Colorado School of Mines.

References

Brandsberg-Dahl, S., O'Brien, M.J., Whitmore, D., Etgen, J.T., & Murphy, G.E. 1999. Multi-component modeling of the Valhall field. *In: EAGE expanded abstract*, vol. 61.

De Hoop, M. V. 1996. Generalization of the Bremmer coupling series. *J. Math. Phys.*, **37**, 3246–3282.

De Hoop, M. V., Le Rousseau, J. H., & Wu, R.-S. 1999. General formulation of screen methods for the scattering of acoustic waves. *Wave Motion, in print*.

De Witte-Morette, C., Maheshwari, A., & Nelson, B. 1979. Path integration in non-relativistic quantum mechanics. *Physics Reports*, **50**, 255–372.

Fishman, L., & McCoy, J.J. 1984a. Derivation and application of extended parabolic wave theories I. The factorized Helmholtz equation. *J. Math. Phys.*, **25**, 285–296.

Fishman, L., & McCoy, J.J. 1984b. Derivation and application of extended parabolic wave theories II. Path integral representations. *J. Math. Phys.*, **25**, 297–308.

Gazdag, J. 1978. wave equation migration with the phase-shift method. *Geophysics*, **43**, 1342–1351.

Hörmander, L. 1985. *The analysis of linear partial differential operator*. Vol. 3. Springer-Verglad, Berlin.

Jones, E.A., & Wang, H.F. 1981. Ultrasonic velocities in Cretacious shales from the williston basin. *Geophysics*, **46**, 288–297.

Le Rousseau, J.H., & De Hoop, M.V. 1999. Modeling and imaging with the scalar generalized-screen algorithms in isotropic media. *Geophysics, submitted*.

Ratcliffe, J.A. 1956. Some aspects of diffraction theory and their application to the ionosphere. *Rep. Prog. Phys.*, **19**, 190–263.

Schoenberg, M., & De Hoop, M.V. 1999. Approximate dispersion relations for qP-qSV waves in transversely isotropic media. *Geophysics, in print*.

Stoffa, P. L., Fokkema, R. M., de Luna Freire, & Kessinger, W. P. 1990. Split-step Fourier Migration. *Geophysics*, **55**, 410–421.

Thomsen, L. 1986. Weak elastic anisotropy. *Geophysics*, **51**, 1954–1966.

Thomsen, L. 1998. *personal communication*.

Thomsen, L.A., Barkved, O., Haggard, B., Kommedal, J.H., & Rosland, B. 1997. Converted-wave imaging of Valhall reservoir. *In: EAGE expanded abstract*, vol. 59.

Treves, F. 1980. *Introduction to pseudodifferential and Fourier integral operators*. Vol. 1. Plenum Press, New York.

Tsvankin, I. 1995. P-wave signatures and notation for transvesely isotropic media: an overview. *Geophysics*, **61**(2), 467–483.

FIGURE CAPTIONS

FIG. 1. Principal parts of the generalized-screen vertical slowness, as a function of the horizontal slowness p, in the elliptical VTI case ($\varepsilon = 0.3$, $\delta = 0.3$) in a constant-wave speed perturbation medium: zero-order (GSP0), first-order (GSP1) and second-order (GSP2).

FIG. 2. Principal parts of the generalized-screen vertical slowness, as a function of the horizontal slowness p, in the VTI case ($\varepsilon = 0.2$, $\delta = 0.0$) in a constant-wave speed perturbation medium: zero-order (GSP0), first-order (GSP1) and second-order (GSP2).

FIG. 3. Principal parts of the generalized-screen vertical slowness, as a function of the horizontal slowness p, in the VTI case in a constant-ε perturbation medium: zero-order (GSP0) and first-order (GSP1).

FIG. 4. Principal parts of the generalized-screen vertical slowness, as a function of the horizontal slowness p, in the VTI case in a constant-δ perturbation medium: zero-order (GSP0) and first-order (GSP1).

FIG. 5. Wavefronts in a constant-wave speed perturbation VTI medium ($\varepsilon = 0.3$, $\delta = 0.3$) associated with the various generalized-screen approximations: second-order (GSP2), first-order (GSP1); top: as calculated as polar reciprocal of the slowness surface; bottom: numerical wavefront.

FIG. 6. Wavefronts in a constant-wave speed perturbation VTI medium ($\varepsilon = 0.2$, $\delta = 0.0$) associated with the various generalized-screen approximations: second-order (GSP2), first-order (GSP1); top: as calculated as polar reciprocal of the slowness surface; bottom: numerical wavefront.

FIG. 7. Wavefronts in a constant-ε perturbation VTI medium associated with the first-order(GSP1) approximation; top: as calculated as polar reciprocal of the slowness surface; bottom: numerical wavefront.

FIG. 8. Wavefronts in a constant-δ perturbation VTI medium associated with the first-order(GSP1) approximation; top: as calculated as polar reciprocal of the slowness surface; bottom: numerical wavefront.

FIG. 9. Vertical wavespeed of the VTI model of the Valhall field. The asterisk locates the position of the source; the dashed line indicates the region detailed in Figure 12 and Figure 13.

FIG. 10. Model for ε of the VTI model of the Valhall field.

FIG. 11. Model for δ of the VTI model of the Valhall field.

FIG. 12. Snapshot of the wavefield in the Valhall model at time $t = 1.6$ s of the pressure field with the full elastic wave equation.

FIG. 13. Snapshot of the wavefield in the Valhall model at time $t = 1.6$ s with the second order of the generalized-screen method.

FIG. 14. Relative error between the approximate phase velocity as given by dispersion relation (11) and the exact phase velocity as a function of the phase angle θ, in the case of Greenhorn shale.

FIG. 15. Gray curve: exact polarization angle (gray curve) as a function of the phase angle θ, in the case of Greenhorn shale; black curve: Error in degrees between the approximate polarization angle as given equation (A-33) and the exact polarization angle.

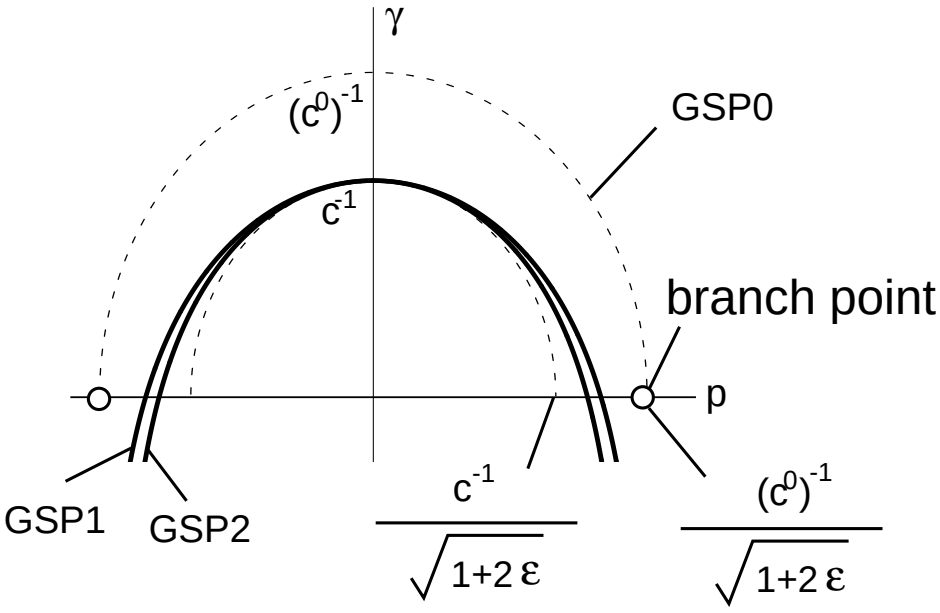
γ
$(c^0)^{-1}$
GSP0
c^{-1}
branch point
p
GSP1
GSP2
$\frac{c^{-1}}{\sqrt{1+2\varepsilon}}$
$\frac{(c^0)^{-1}}{\sqrt{1+2\varepsilon}}$

FIG. 1.

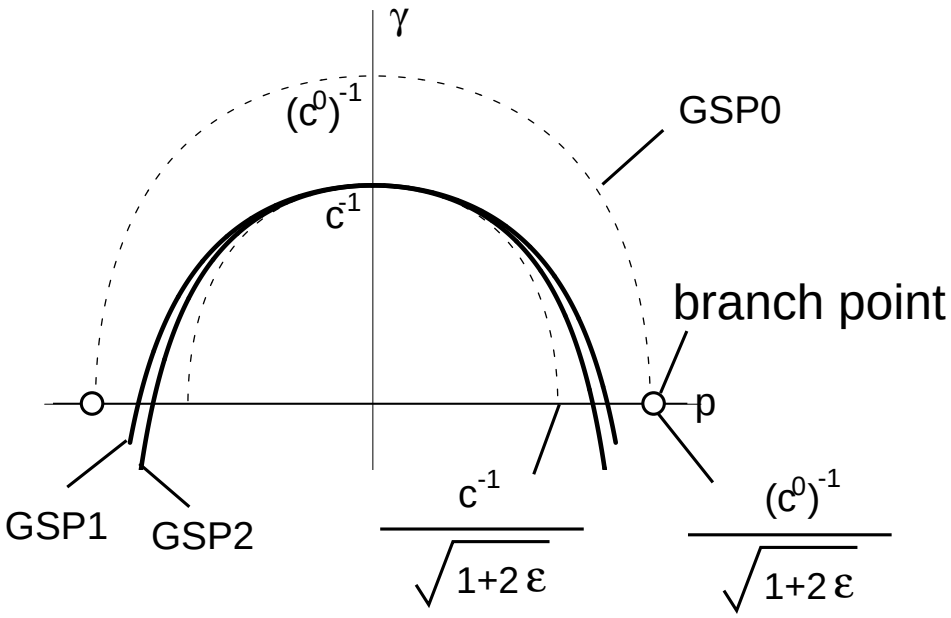
γ
$(c^0)^{-1}$
GSP0
c^{-1}
branch point
p
GSP1
GSP2
$\frac{c^{-1}}{\sqrt{1+2\varepsilon}}$
$\frac{(c^0)^{-1}}{\sqrt{1+2\varepsilon}}$

FIG. 2.

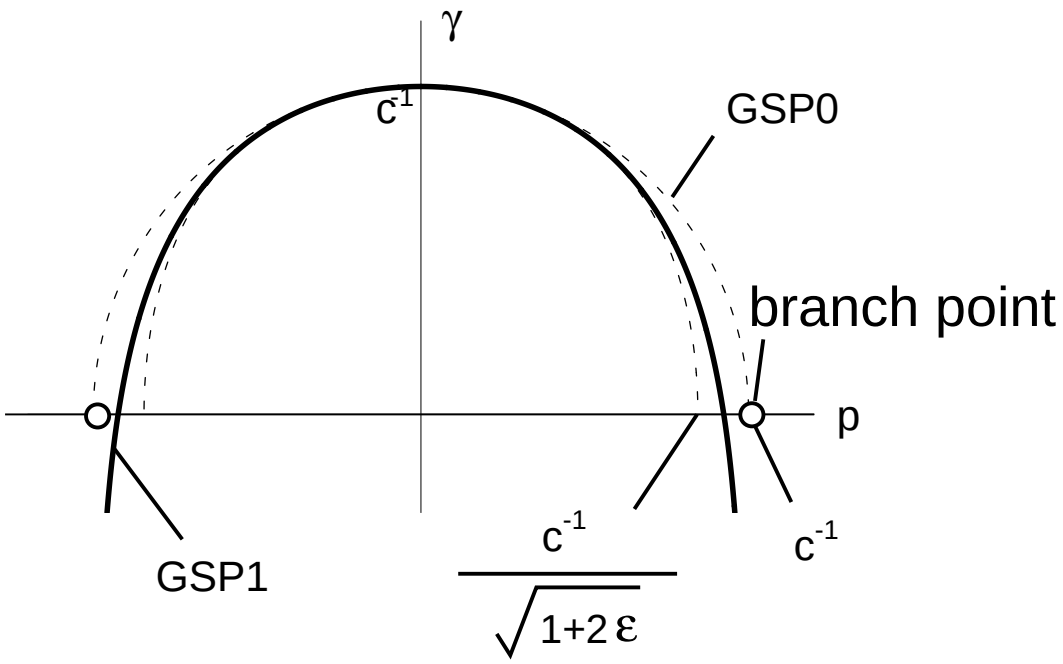

FIG. 3.

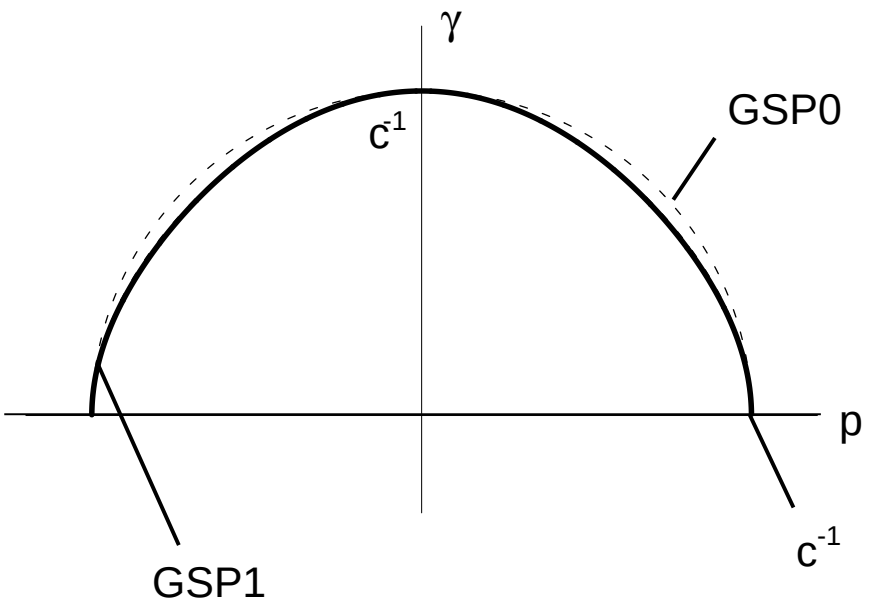

FIG. 4.

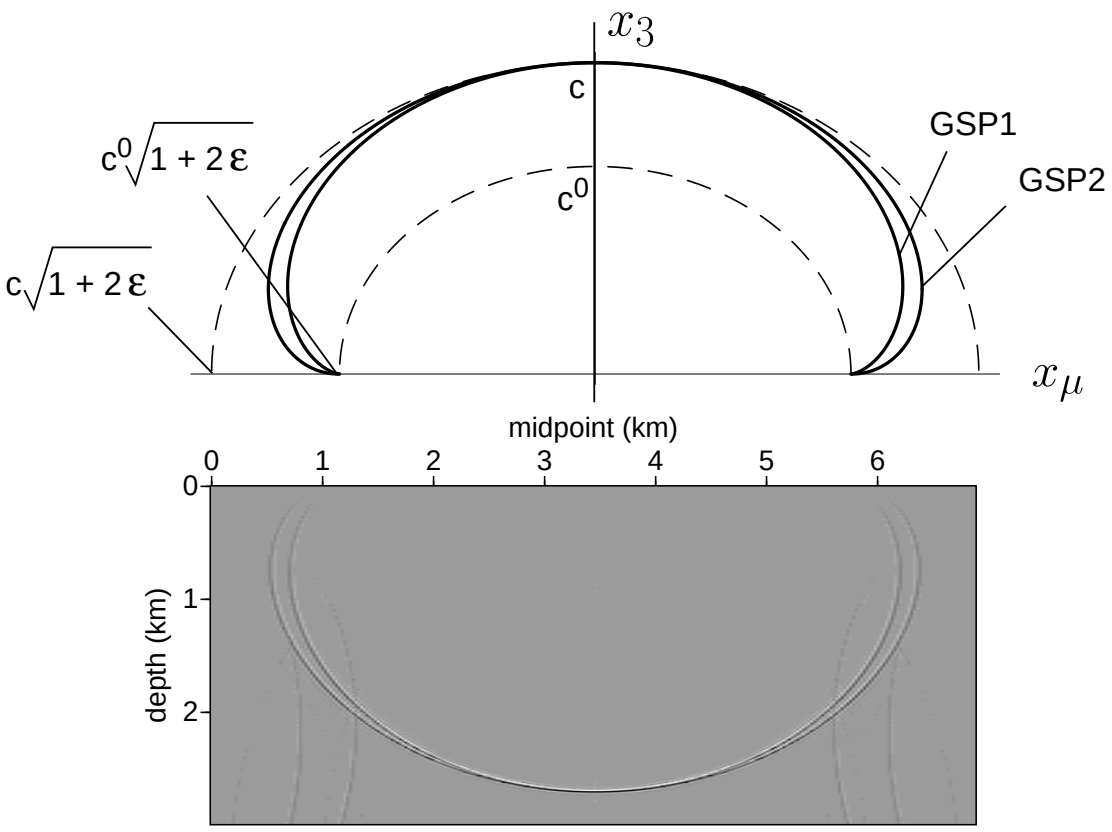
x_3
c
$c^0\sqrt{1+2\varepsilon}$
c^0
GSP1
GSP2
$c\sqrt{1+2\varepsilon}$
x_μ
midpoint (km)
0
1
2
3
4
5
6
depth (km)
0
1
2

FIG. 5.

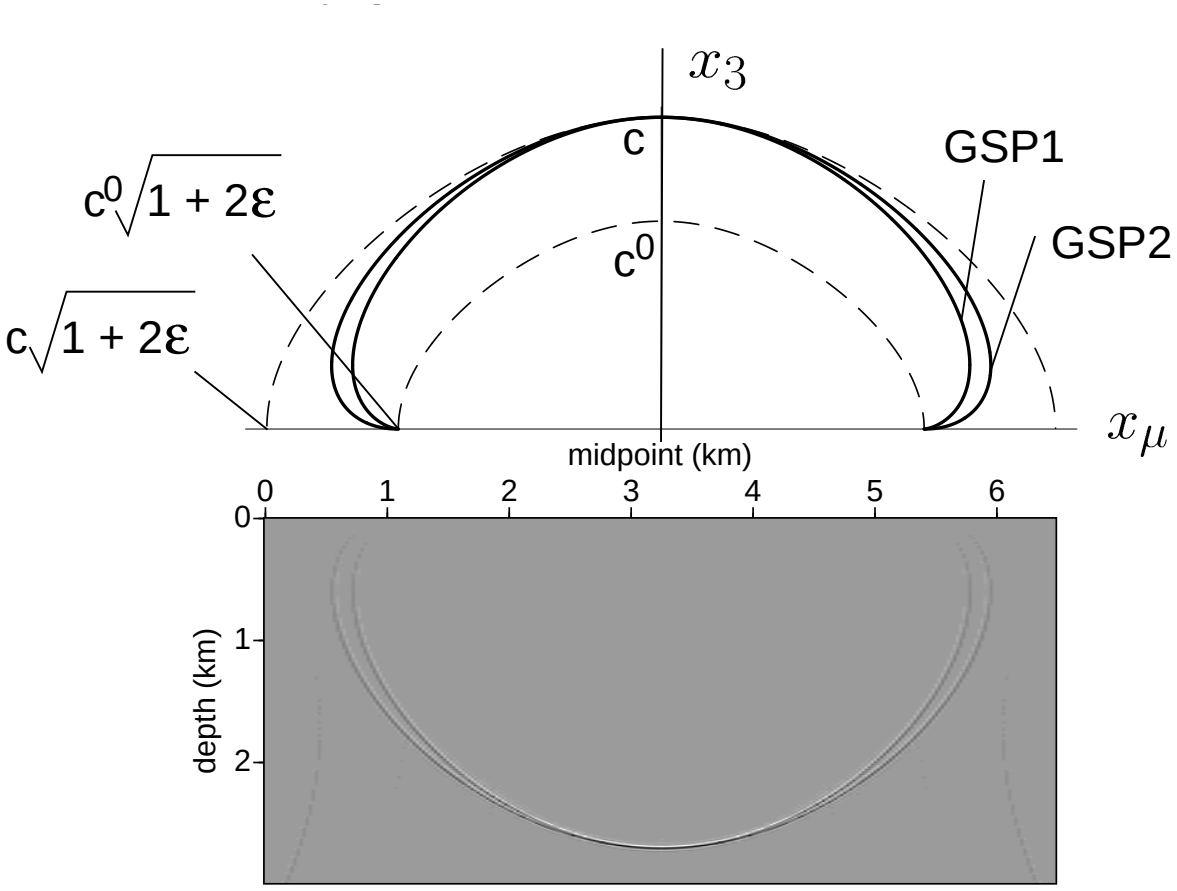
x_3
c
GSP1
GSP2
$c^0\sqrt{1+2\varepsilon}$
c^0
$c\sqrt{1+2\varepsilon}$
x_μ
midpoint (km)
0
1
2
3
4
5
6
depth (km)
0
1
2

FIG. 6.

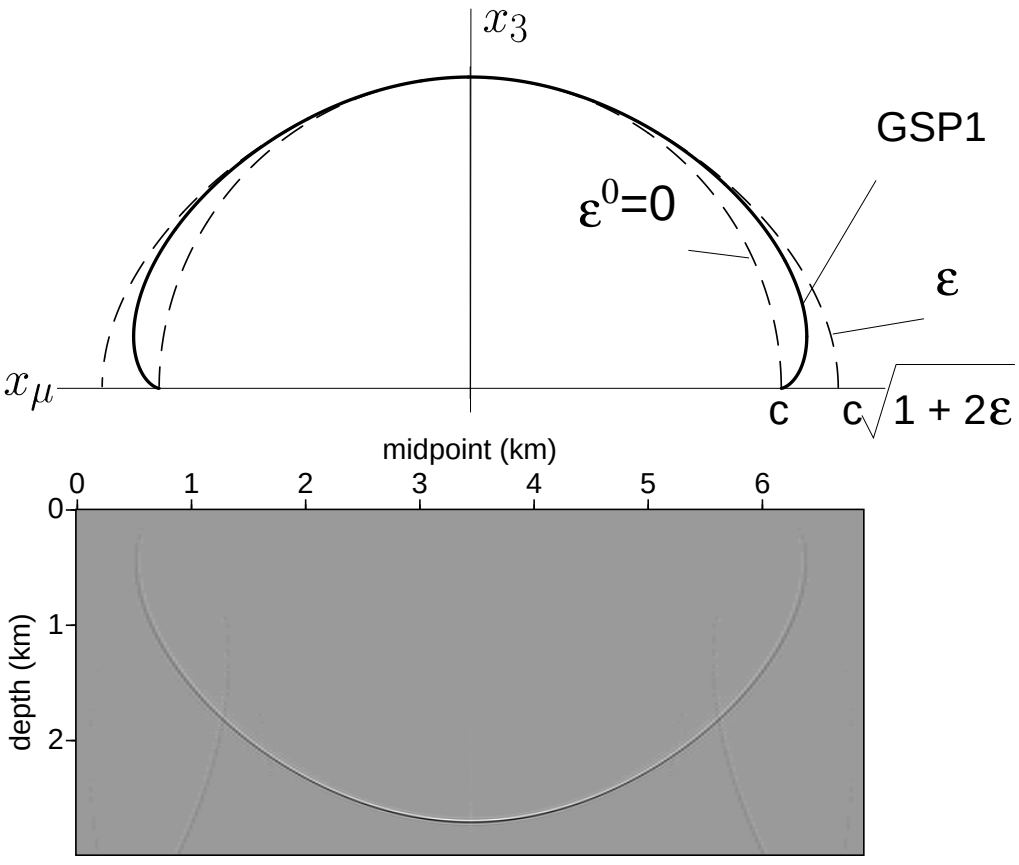
x_3
GSP1
$\varepsilon^0=0$
ε
x_μ
c
c$\sqrt{1+2\varepsilon}$
midpoint (km)
0
1
2
3
4
5
6
depth (km)
0
1
2

FIG. 7.

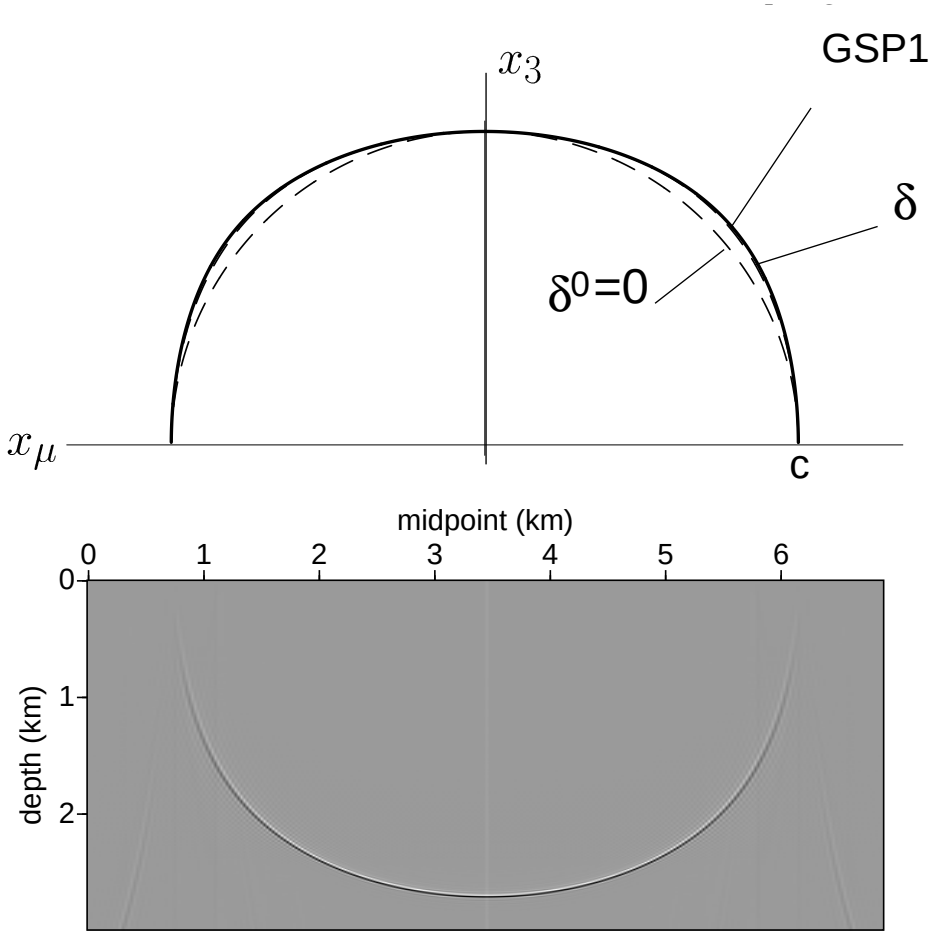

FIG. 8.

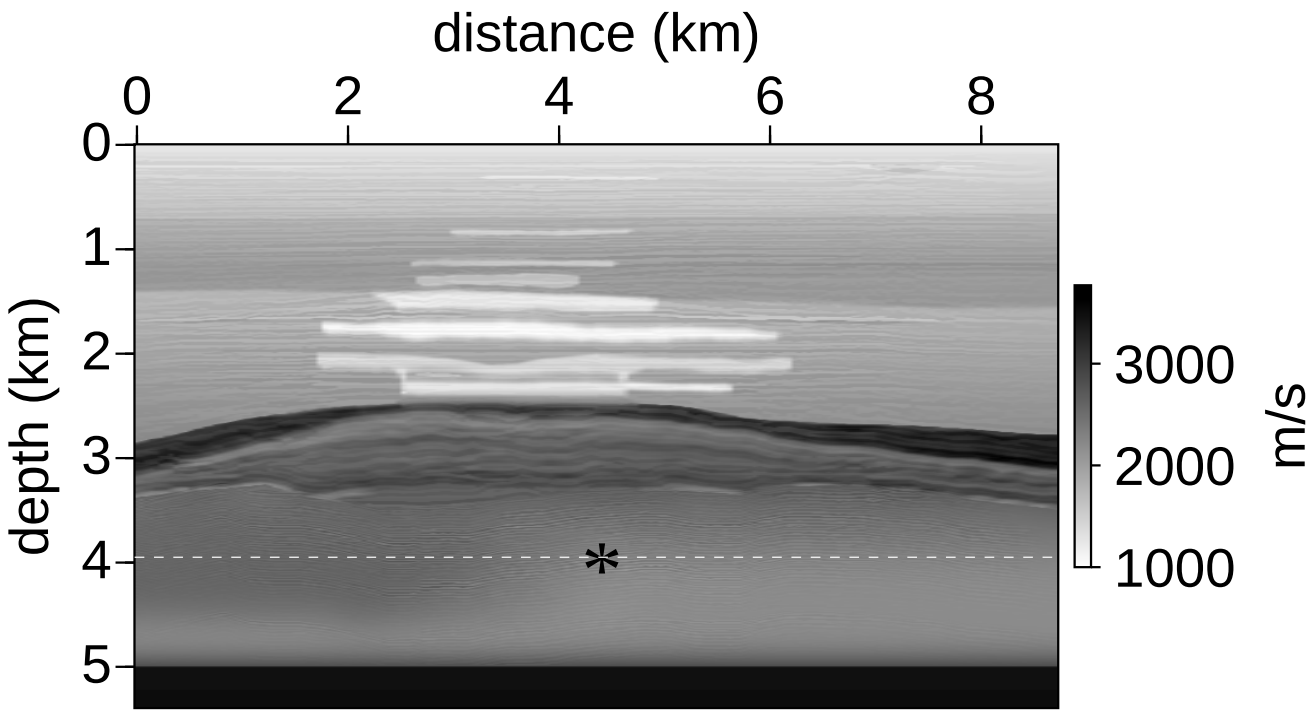

FIG. 9.

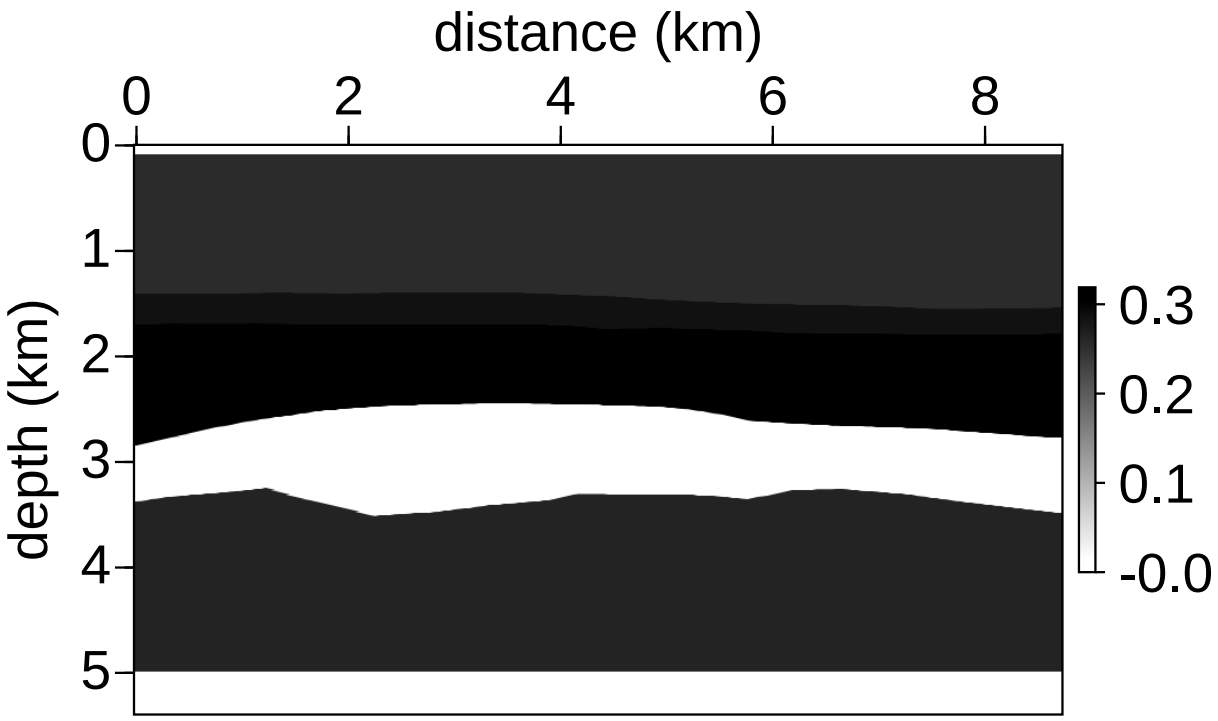

FIG. 10.

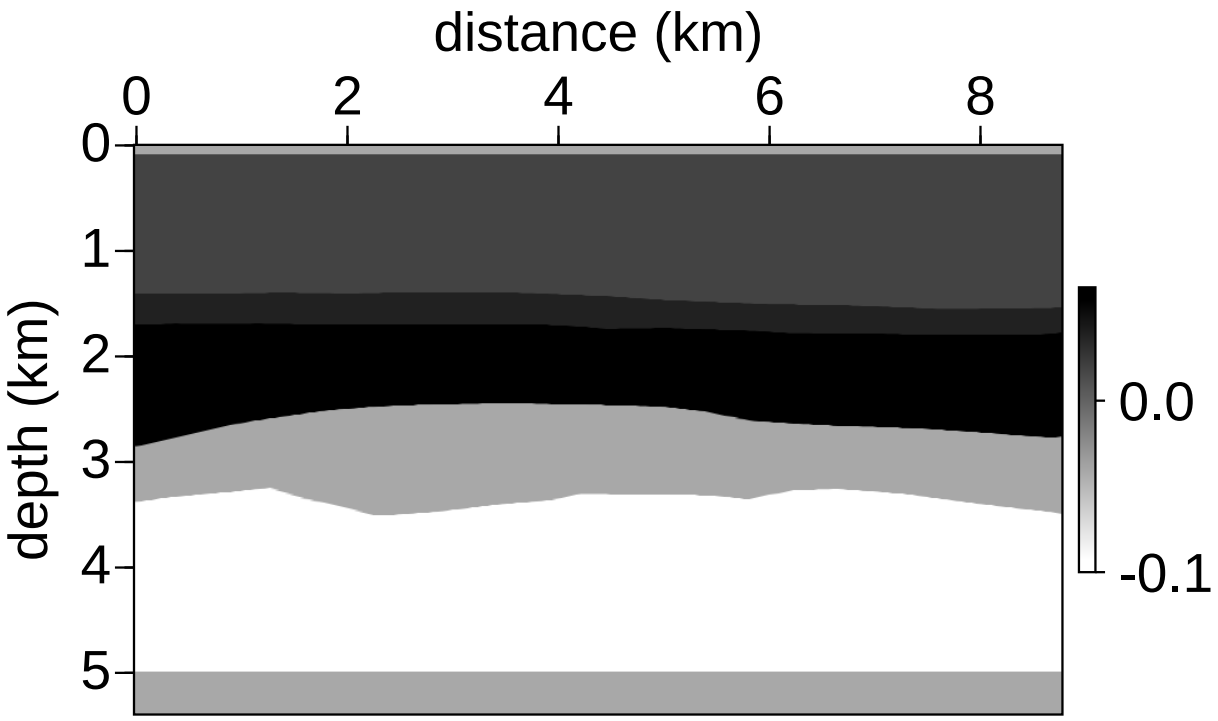

FIG. 11.

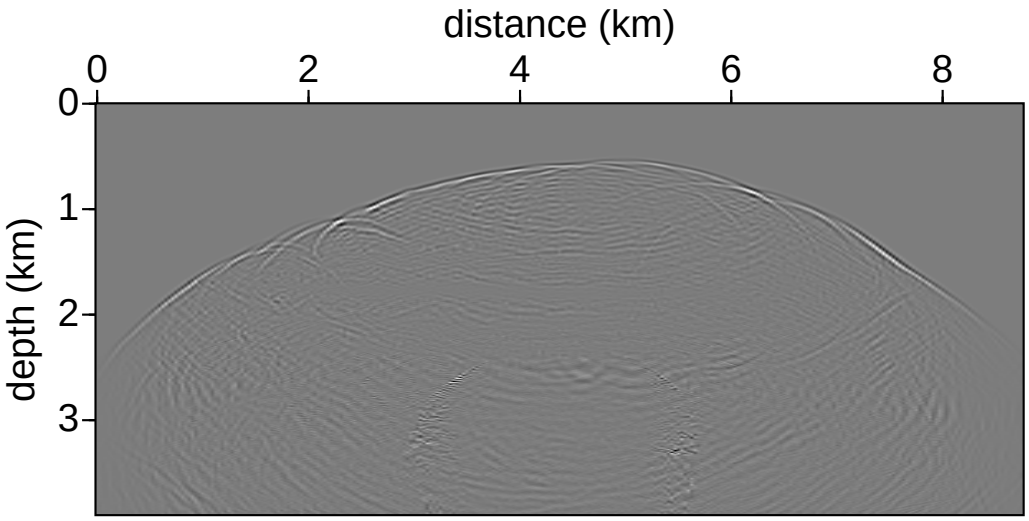

FIG. 12.

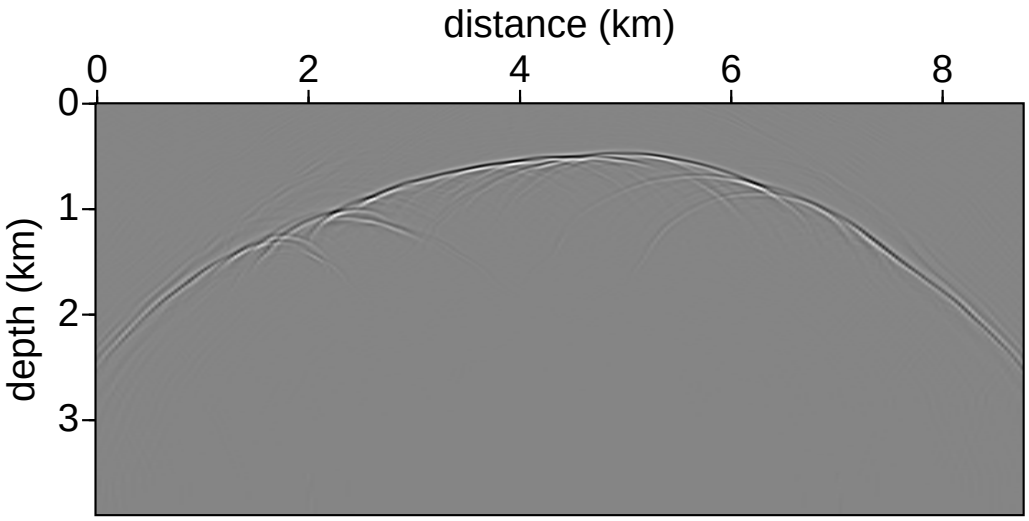

FIG. 13.

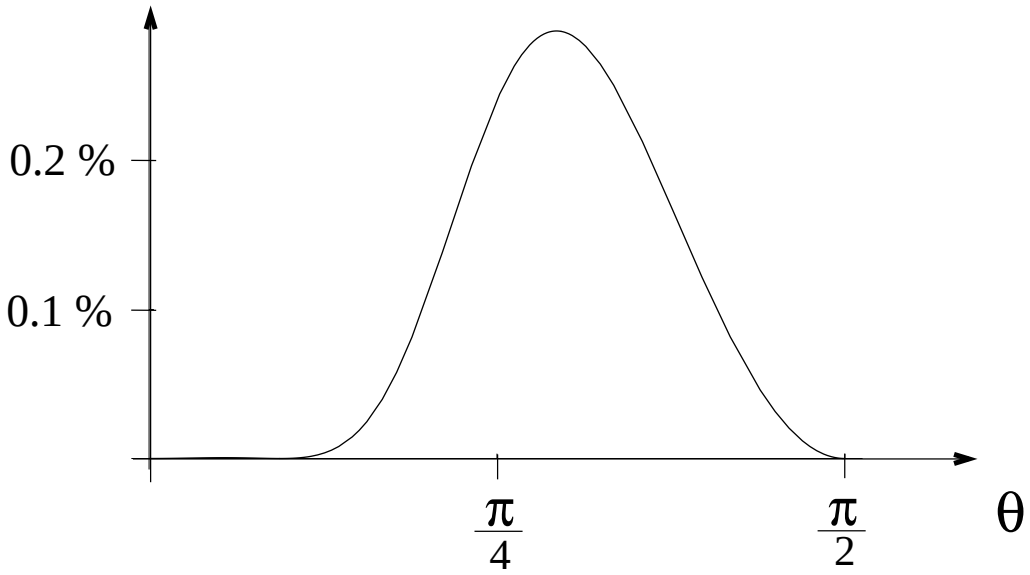

FIG. 14.

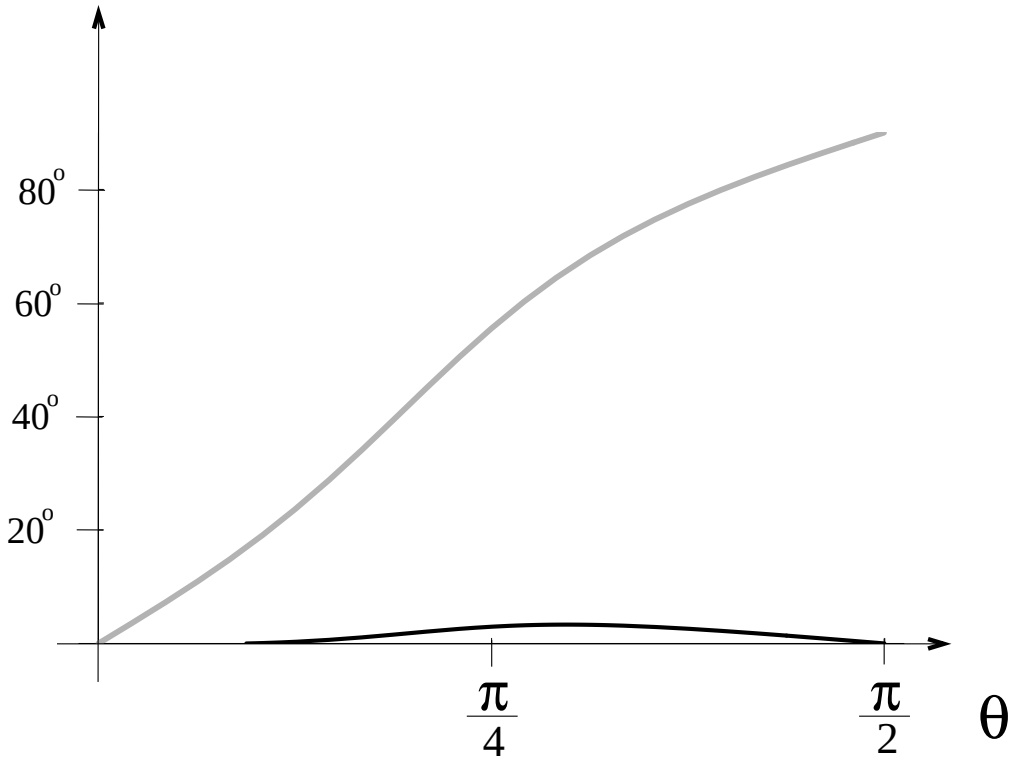

FIG. 15.

APPENDIX A: EQUIVALENT 'ACOUSTIC' SYSTEM OF EQUATIONS FOR VTI QP-WAVE PROPAGATION

VTI media are essentially elastic media. Yet, in various applications the propagation of qP-wave only is treated, as if the medium were acoustic. Here, we propose to derive an equivalent 'acoustic' system of equations for the VTI media characterized by 'mild' anisotropy (Schoenberg & De Hoop, 1999).

Exact VTI system and limiting equivalent 'acoustic' system

The medium being VTI, we work in a vertical plane without loss of generality. In an elastic medium, the wave equation is given by the second-order hyperbolic system

$$\rho\partial_t^2 u_i - \partial_j \left(C_{ijkl}\partial_l u_k\right) = f_i \ , \ \text{for} \ \ i = 1, 3, \tag{A-1}$$

where u_i=particle displacement (m), ρ=volume density of mass (kg/m^3), C_{ijkl}=stiffness tensor (Pa), and f_i=volume source density of force (N/m^3). In the VTI case, system (A-1) reduces to

$$\rho\partial_t^2 u_1 - \partial_1 \left(c_{11}\partial_1 u_1 + c_{13}\partial_3 u_3\right) - \partial_3 \left(c_{55}(\partial_3 u_1 + \partial_1 u_3)\right) = f_1 \ , \tag{A-2}$$

$$\rho\partial_t^2 u_3 - \partial_3 \left(c_{13}\partial_1 u_1 + c_{33}\partial_3 u_3\right) - \partial_1 \left(c_{55}(\partial_3 u_1 + \partial_1 u_3)\right) = f_3 \ , \tag{A-3}$$

according to the stiffness matrix (1) and the Voigt notation.

Let $a = c_{13} + 2c_{55}$ be fixed. Following Schoenberg and De Hoop (1999), we artificially modify the stiffness coefficients according to:

$$c_{13} \to a \ , \tag{A-4}$$

$$c_{55} \to 0 \ . \tag{A-5}$$

Taking the vertical qSV-wave speed equal to zero yields an equivalent 'acoustic' system; however, as noticed by Schoenberg and De Hoop (1999), keeping $c_{13} + 2c_{55}$ constant, as is done

here, does not affect dramatically the shape of the qP-slowness surface in the case of 'mild' anisotropy. The second-order system (A-2)-(A-3) thus becomes

$$\rho\partial_t^2 u_1 - \partial_1 \left(c_{11}\partial_1 u_1 + a\partial_3 u_3\right) = f_1 \ , \tag{A-6}$$

$$\rho\partial_t^2 u_3 - \partial_3 \left(a\partial_1 u_1 + c_{33}\partial_3 u_3\right) = f_3 \ . \tag{A-7}$$

We define a pseudo-pressure, p, as

$$p \equiv - \left(a\partial_1 u_1 + c_{33}\partial_3 u_3\right) \ . \tag{A-8}$$

Then equation (A-7) takes the form

$$\rho\partial_t^2 u_3 + \partial_3 p = f_3 \ , \tag{A-9}$$

which equation appears in the isotropic acoustic case also (De Hoop, 1996, equation (II.6)). From equation (A-8) one can extract $\partial_3 u_3$,

$$\partial_3 u_3 = -\frac{1}{c_{33}} p - \frac{a}{c_{33}}\partial_1 u_1 \ , \tag{A-10}$$

which upon substitution in equation (A-6) yields

$$\left\{\rho\partial_t^2 - \partial_1 \left[\left(c_{11} - \frac{a^2}{c_{33}}\right)\partial_1 \cdot\right]\right\} u_1 + \partial_1 \left(\frac{a}{c_{33}} \cdot\right) p = f_1 \ , \tag{A-11}$$

which we rewrite as

$$O\, u_1 + \partial_1 \left(\frac{a}{c_{33}} \cdot\right) p = f_1 \ , \tag{A-12}$$

with

$$O(\partial_t, \partial_1) = \rho\partial_t^2 - \partial_1 \left[\left(c_{11} - \frac{a^2}{c_{33}}\right)\partial_1 \cdot\right] \ . \tag{A-13}$$

The principal part, O_2, of the differential operator O is given by

$$O_2(\partial_t, \partial_1) = \rho\partial_t^2 - \left(c_{11} - \frac{a^2}{c_{33}}\right)\partial_1^2 \ , \tag{A-14}$$

and its principal symbol, o_2, follows, upon replacing ∂_t and ∂_1 by their respective symbols, s^2 and $-\mathrm{i}s\alpha$, in the Laplace-Fourier domain, as

$$o_2(s,\alpha) = \rho s^2 + \left(c_{11} - \frac{a^2}{c_{33}}\right)\alpha^2 \ . \tag{A-15}$$

In the case where $a^2 < c_{11}c_{33}$, which we assume[2] here, the differential operator O is strongly elliptic. We can therefore invert it (Treves, 1980), and hence with equation (A-12),

$$u_1 = -O^{-1}\left[\partial_1\left(\frac{a}{c_{33}}\,\cdot\right)\right]p + O^{-1}f_1 \ . \tag{A-16}$$

Substituting equation (A-16) into the definition (A-8) of the pseudo-pressure, p, we obtain

$$\partial_3 u_3 + \left\{\frac{1}{c_{33}} - \frac{a}{c_{33}}\partial_1\, O^{-1}\left[\partial_1\left(\frac{a}{c_{33}}\,\cdot\right)\right]\right\}p = -\frac{a}{c_{33}}\partial_1 O^{-1} f_1 \ . \tag{A-17}$$

Using the particle velocity, $\boldsymbol{v}$, instead of the particle displacement, $\boldsymbol{u}$, we obtain the system of equations

$$\rho\partial_t v_3 + \partial_3 p \ = \ f_3 \ , \tag{A-18}$$

$$\partial_3 v_3 + \left\{\frac{1}{c_{33}} - \frac{a}{c_{33}}\partial_1\, O^{-1}\left[\partial_1\left(\frac{a}{c_{33}}\,\cdot\right)\right]\right\}\partial_t p \ = \ -\frac{a}{c_{33}}\partial_1\, O^{-1}\partial_t f_1 \ . \tag{A-19}$$

Defining the 'acoustic' field matrix, F_I, I=1,3, as

$$F_1 \ = \ p \ , \tag{A-20}$$

$$F_3 \ = \ v_3 \ , \tag{A-21}$$

we obtain the matrix differential equation

$$(\partial_3\delta_{I,J} + A_{I,J}\partial_t)F_J = N_I \ , \tag{A-22}$$

where the elements of the acoustic system operator matrix, $A_{I,J}$, are given by

$$A_{1,1} \ = \ 0 \ , \tag{A-23}$$

[2]Note that the case $a^2 > c_{11}c_{33}$ would induce a pole in expression (A-31) for the vertical slowness γ_1, i.e. the phase velocity would have a zero.

$$A_{1,2} = \rho \, , \tag{A-24}$$

$$A_{2,1} = \left\{ \frac{1}{c_{33}} - \frac{a}{c_{33}} \partial_1 \, O^{-1} \left[\partial_1 \left(\frac{a}{c_{33}} \cdot \right) \right] \right\} \, , \tag{A-25}$$

$$A_{2,2} = 0 \, . \tag{A-26}$$

The source matrix, N_I, $I = 1, 3$, is given by

$$N_1 = f_3 \, , \tag{A-27}$$

$$N_3 = -\frac{a}{c_{33}} \partial_1 \, O^{-1} \partial_t f_1 \, . \tag{A-28}$$

Observe that in the limiting case $c_{11} = c_{33} = a$, we recover the exact form of the acoustic-matrix differential equation for an isotropic-acoustic medium (De Hoop, 1996, equations (II-9) through (II-16)); then the linear operator O reduces to $\rho \, \partial_t^2$.

Dispersion relation for the equivalent 'acoustic' system

To obtain the dispersion relation, i.e., to derive the (micro-local) eikonal equation, we consider a (locally) constant medium ('high-frequency' approximation). Then the linear operator O reduces to its principal part O_2. Upon applying a Fourier transform in the spatial coordinates, x_1 and x_3, and a Laplace transform in time, t, to system (A-22) thus replacing ∂_t, ∂_3, ∂_1, and O_2 by their respective symbols, s^2, $-s\gamma_1$, $-\mathrm{i}s\alpha$, and o_2, we set the determinant of system (A-22) equal to zero:

$$\rho s^2 \left[\frac{a^2}{c_{33}^2} o_2^{-1} s^2 \alpha^2 + \frac{1}{c_{33}} \right] - s^2 \gamma_1^2 = 0 \, , \tag{A-29}$$

which can be written as

$$\gamma_1^2 = \frac{\frac{\tilde{a}^2}{\tilde{c}_{33}^2} \alpha^2}{1 + \tilde{c}_{11} \alpha^2 - \frac{\tilde{a}^2}{\tilde{c}_{33}} \alpha^2} + \frac{1}{\tilde{c}_{33}} \, . \tag{A-30}$$

Note that the term $\tilde{c}_{ij}$ represents the elastic moduli c_{ij} normalized by density, ρ. The previous equation simplifies to

$$\gamma_1^2 = \frac{1 + \tilde{c}_{11} \alpha^2}{\tilde{c}_{33} \left(1 + \left(1 - \frac{\tilde{a}^2}{\tilde{c}_{11} \tilde{c}_{33}} \right) \alpha^2 \right)} \, , \tag{A-31}$$

which yields

$$\left[1-\left(1-\frac{\tilde{a}^2}{\tilde{c}_{11}\tilde{c}_{33}}\right)X\right]Z=1-X\ , \tag{A-32}$$

when carrying out the change of variables (7). The dispersion relation defines the slowness surface (γ_1 as a function of $-\mathrm{i}\alpha$), and hence the phase velocity, as the reciprocal of the slowness. Figure 14 illustrates the relative error between the approximate phase velocity given by equation (11) and the exact dispersion relation using the measured moduli of Greenhorn shale (Jones & Wang, 1981); the stiffness coefficients in $(\mathrm{km/s})^2$ are

$$c_{11}=14.47\ ,\quad c_{33}=9.57\ ,\quad c_{55}=2.28\ ,\quad c_{13}=4.51\ .$$

Polarization angle

Here, we study the (micro-local) behavior of the polarization vector. Upon applying a Fourier transform in the spatial coordinates, x_1 and x_3, and a Laplace transform in time, t, to system (A-22) thus replacing ∂_t, ∂_3, and ∂_1 by their respective symbols, s^2, $-s\gamma_1$, and $-\mathrm{i}s\alpha$, we can derive the polarization angle, Υ, of the qP-wave in the framework of the approximation proposed by Schoenberg and De Hoop (1999)

$$\tan\Upsilon=\frac{u_1}{u_3}=\frac{\mathrm{i}\alpha\gamma_1\tilde{a}}{1+\tilde{c}_{11}\alpha^2}\ . \tag{A-33}$$

Note that the polarization angle given by equation (A-33) is the limit of the exact polarization angle in VTI media for the qP-wave (e.g., Tsvankin, 1995, equation (42)) when applying transformations (A-4) and (A-5). In the current notation, the exact polarization angle is indeed given by

$$\tan\Upsilon^e=\frac{(\tilde{c}_{13}+\tilde{c}_{55})\mathrm{i}\alpha\gamma_1}{1+\tilde{c}_{11}\alpha^2-\tilde{c}_{55}\gamma_1^2}\ . \tag{A-34}$$

Figure 15 illustrates the degree of accuracy offered by the approximation proposed by Schoenberg and De Hoop (1999) for the polarization angle in the case of Greenhorn shale (Jones & Wang, 1981).

From the value of the polarization angle in the 'mild' anisotropy approximation, Υ, we can recover the exact polarization angle, Υ^e, as

$$\tan \Upsilon^e = \frac{(c_{13} + c_{55})\mathrm{i}\alpha\gamma_1^e}{\mathrm{i}\alpha a\gamma_1 - c_{55}(\gamma_1^e)^2 \tan \Upsilon} \tan \Upsilon \ , \tag{A-35}$$

where γ_1^e is the vertical slowness principal symbol in the exact VTI case. Using the fact that $\gamma_1 \simeq \gamma_1^e$, i.e. that the dispersion relation is weakly affected by the present approximation, this relation simplifies to

$$\tan \Upsilon^e = \frac{(c_{13} + c_{55})\mathrm{i}\alpha}{\mathrm{i}\alpha a - c_{55}\gamma_1 \tan \Upsilon} \tan \Upsilon \ . \tag{A-36}$$

The fractional term can be shown to be quasi insensitive to transformations (A-4) and (A-5) in the case of 'mild' anisotropy.

APPENDIX B: DIRECTIONAL DECOMPOSITION OF THE WAVEFIELD IN THE 'ACOUSTIC' VTI CASE. CHARACTERISTIC EQUATION FOR THE VERTICAL SLOWNESS OPERATOR

To achieve a directional decomposition of the wavefield, we diagonalize system (A-22). We use the one-sided Laplace transform. To show the notation, we give the expression for the pseudo-pressure,

$$\hat{p}(\boldsymbol{x}, s) = \int_0^\infty \exp(-st)\, p(\boldsymbol{x}, t)\, \mathrm{d}t \ . \tag{B-1}$$

In the main text, we omit the hat (ˆ) on the fields and operators in the Laplace domain because there is no confusion possible. We write

$$\hat{F}_I = \hat{L}_{I,J}\hat{W}_J \ , \tag{B-2}$$

where $\hat{W}_I$ is the wave matrix and $\hat{W}_1$ and $\hat{W}_2$ will correspond to the down- and upgoing wave constituents. Note that the elements of the wave matrix, $\hat{W}_I$, may be physically 'non-observable'. We call $\hat{L}_{I,J}$ the composition operator. Substituting the composition equation (B-2) into the matrix differential equation (A-22), we thus obtain the following system of equations

$$\partial_3 \hat{L}_{1,J}\hat{W}_J + s\hat{A}_{1,2}\hat{L}_{2,J}\hat{W}_J \ = \ \hat{N}_1 \ , \tag{B-3}$$

$$s\hat{A}_{2,1}\hat{L}_{1,J}\hat{W}_J + \partial_3\hat{L}_{2,J}\hat{W}_J \;=\; \hat{N}_2 \;. \tag{B-4}$$

We introduce the commutator notation,

$$\left[\partial_3, \hat{L}_{I,J}\right] = \partial_3\hat{L}_{I,J} - \hat{L}_{I,J}\partial_3 \;, \tag{B-5}$$

and obtain

$$\hat{L}_{1,J}\partial_3\hat{W}_J + s\hat{A}_{1,2}\hat{L}_{2,J}\hat{W}_J \;=\; -\left[\partial_3, \hat{L}_{1,J}\right]\hat{W}_J + \hat{N}_1 \;, \tag{B-6}$$

$$s\hat{A}_{2,1}\hat{L}_{1,J}\hat{W}_J + \hat{L}_{2,J}\partial_3\hat{W}_J \;=\; -\left[\partial_3, \hat{L}_{2,J}\right]\hat{W}_J + \hat{N}_2 \;. \tag{B-7}$$

We shall construct the appropriate linear operator, $\hat{L}_{I,J}$, such that the left-hand side of this system attains the form

$$\hat{L}_{I,J}\left(\partial_3\delta_{J,M} + s\hat{\Lambda}_{J,M}\right)\hat{W}_M = -\left[\partial_3, \hat{L}_{I,J}\right]\hat{W}_J + \hat{N}_I \;, \tag{B-8}$$

with the linear operator $\hat{\Lambda}_{I,J}$ being diagonal. The diagonal entries of $\partial_3\delta_{J,M} + s\hat{\Lambda}_{J,M}$ are the up- and downgoing one-way wave operators. The wave matrix, $\hat{W}_I$, and the source matrix, $\hat{N}_I$, being arbitrary, the introduced linear operators, $\hat{L}_{I,J}$ and $\hat{\Lambda}_{I,J}$, have then to satisfy the following system of equations:

$$\hat{A}_{1,2}\hat{L}_{2,1} \;=\; \hat{L}_{1,1}\hat{\Lambda}_{1,1} \;, \tag{B-9}$$

$$\hat{A}_{1,2}\hat{L}_{2,2} \;=\; \hat{L}_{1,2}\hat{\Lambda}_{2,2} \;, \tag{B-10}$$

$$\hat{A}_{2,1}\hat{L}_{1,1} \;=\; \hat{L}_{2,1}\hat{\Lambda}_{1,1} \;, \tag{B-11}$$

$$\hat{A}_{2,1}\hat{L}_{1,2} \;=\; \hat{L}_{2,2}\hat{\Lambda}_{2,2} \;. \tag{B-12}$$

Let the diagonal entries of $\hat{\Lambda}_{I,J}$ be denoted as

$$\hat{\Lambda}_{1,1} \;=\; \hat{\Gamma}^{(+)} \;,$$

$$\hat{\Lambda}_{2,2} \;=\; \hat{\Gamma}^{(-)} \;.$$

We apply the acoustic-pressure normalization analog introduced by De Hoop (1996), to obtain the Ansatz:

$$\hat{L}_{1,1} = \hat{A}_{1,2} \,, \tag{B-13}$$

$$\hat{L}_{2,1} = \hat{\Gamma}^{(+)} \,, \tag{B-14}$$

$$\hat{L}_{1,2} = \hat{A}_{1,2} \,, \tag{B-15}$$

$$\hat{L}_{2,2} = \hat{\Gamma}^{(-)} \,. \tag{B-16}$$

Equations (B-9) and (B-10) are then satisfied and equations (B-11) and (B-12) yield the following characteristic equations

$$\hat{\Gamma}^{(\pm)}\hat{\Gamma}^{(\pm)} = \hat{\mathrm{A}} = \hat{A}_{2,1}\hat{A}_{1,2} \,. \tag{B-17}$$

The differential operator $\hat{\mathrm{A}}$ is called the transverse Helmholtz operator and is given by

$$\hat{\mathrm{A}} = \left\{ \frac{1}{c_{33}}\rho - \frac{a}{c_{33}}\partial_1 \hat{O}^{-1} \left[\partial_1 \left(\frac{a}{c_{33}}\rho \, \cdot \right) \right] \right\} \,. \tag{B-18}$$

In view of the up-down symmetry of the medium, the solutions of equation (B-17) are written as

$$\hat{\Gamma}^{(+)} = -\hat{\Gamma}^{(-)} = \hat{\Gamma} = \hat{\mathrm{A}}^{\frac{1}{2}} \,. \tag{B-19}$$

The composition operator thus becomes

$$\hat{L} = \begin{pmatrix} \hat{A}_{1,2} & \hat{A}_{1,2} \\ \hat{\Gamma} & -\hat{\Gamma} \end{pmatrix} \,, \tag{B-20}$$

and its inverse, the decomposition operator, $\hat{L}^{-1}$, then follows as

$$\hat{L}^{-1} = \frac{1}{2} \begin{pmatrix} \hat{A}_{1,2}^{-1} & \hat{\Gamma}^{-1} \\ \hat{A}_{1,2}^{-1} & -\hat{\Gamma}^{-1} \end{pmatrix} \,. \tag{B-21}$$

The elements of the wave matrix, $\hat{W}_I$, correspond with the pseudo-pressure up the action of $\hat{A}_{1,2}$.

Using the Fourier transform with respect to the horizontal spatial coordinates we can associate with $\hat{\Gamma}$ and $\hat{\mathrm{A}}$ their 'left symbols' (Hörmander, 1985; Treves, 1980), $\hat{\gamma}$ and $\hat{\mathrm{a}}$ respectively, i.e., let $\hat{\phi}$ be a test function, then

$$(\hat{\Gamma}\hat{\phi})(x_\mu, x_3) = \int (s/2\pi)^2 \mathrm{d}\alpha_1 \mathrm{d}\alpha_2 \int \mathrm{d}x_1' \mathrm{d}x_2' \; \hat{\gamma}(x_\mu, x_3; \alpha_\nu) \exp[-\mathrm{i}s(x_\sigma - x_\sigma')\alpha_\sigma] \; \hat{\phi}(x_\upsilon', x_3) \; ,$$

$$(\hat{\mathrm{A}}\hat{\phi})(x_\mu, x_3) = \int (s/2\pi)^2 \mathrm{d}\alpha_1 \mathrm{d}\alpha_2 \int \mathrm{d}x_1' \mathrm{d}x_2' \; \hat{\mathrm{a}}(x_\mu, x_3; \alpha_\nu) \exp[-\mathrm{i}s(x_\sigma - x_\sigma')\alpha_\sigma] \; \hat{\phi}(x_\upsilon', x_3) \; ,$$

The characteristic equation (B-17) transforms into a characteristic equation for left symbols:

$$\exp\left[-\mathrm{i}\,\partial_{\alpha'} D_{x_1'}\right] \; \hat{\gamma}(x_1; \alpha')\hat{\gamma}(x_1'; \alpha)\Big|_{(x_1', \alpha') = (x_1, \alpha)} = \hat{\mathrm{a}}(x_1; \alpha) \; , \tag{B-22}$$

as given by symbol calculus of pseudodifferential operators (Treves, 1980; De Hoop, 1996, equation (A12)). In this paper, we assume the medium to be locally constant, i.e., we apply a 'high-frequency' approximation; then the symbols $\hat{\gamma}$ and $\hat{\mathrm{a}}$ reduce to their principal parts $\hat{\gamma}_1$ and $\hat{\mathrm{a}}_2$ respectively. Up to principal symbols, this characteristic equation thus becomes the dispersion relation

$$\hat{\gamma}_1^2 = \hat{a}_2 = \frac{1 + \tilde{c}_{11}\alpha^2}{\tilde{c}_{33}\left(1 + \left(1 - \frac{\tilde{a}^2}{\tilde{c}_{11}\tilde{c}_{33}}\right)\alpha^2\right)} \; . \tag{B-23}$$

This explains the subscript 1 in $\hat{\gamma}_1$ in the dispersion relation (5). The symbol $\hat{\gamma}_1$ is the vertical component of the slowness vector and hence we can then interpret $\hat{\Gamma}$ as the *vertical slowness* operator.

Finding a equivalent 'acoustic' wave operator in the diagonal form (B-8) characterizing the qP-wave propagation in ('mildly' anisotropic) VTI media, allows then to express the one-way wave propagator as in equation (14) the way it is done in acoustic isotropic media (De Hoop, 1996; De Hoop *et al.*, 1999). The thin-slab propagator is then

$$\hat{g}^{(\pm)}(x_\mu, x_3; x_\upsilon', x_3') \simeq$$

$$\int (s/2\pi)^2 \mathrm{d}\alpha_1 \mathrm{d}\alpha_2 \exp[-\mathrm{i}s\,\alpha_\sigma(x_\sigma - x_\sigma')] \exp[\mp s\,\hat{\gamma}(x_\mu, \bar{x}_3; \alpha_\nu)\Delta x_3] \; . \tag{B-24}$$

In the framework of the 'high-frequency' approximation, $\hat{\gamma}$ reduces to its principal part, $\hat{\gamma}_1$, and the thin-slab propagator reduces to equation (14).

Mapping between acoustic field matrix components and observable

To obtain the equivalent 'acoustic' system, we have used a pseudo-pressure that is not observable. The introduction of p allows a simple wave field decomposition, that is presented in Appendix B. Yet, as given by equation (A-10), we can map the two field matrix components, p and v_3, to the particle velocity according to:

$$v_3 = v_3 \ , \tag{B-25}$$

$$\partial_1 v_1 = -\frac{1}{a}\partial_t p - \frac{c_{33}}{a}\partial_3 v_3 \ , \tag{B-26}$$

with appropriate initial conditions.